C. R. Mecanique 343 (2015) 371–396

Contents lists available at ScienceDirect

Comptes Rendus Mecanique

www.sciencedirect.com

Thermo-mechanical characterization of multi-walled carbon nanotube reinforced polycarbonate composites: A molecular dynamics approach

Sumit Sharma [a,*,1], Rakesh Chandra [b,2], Pramod Kumar [b,3], Navin Kumar [c,2]

[a] School of Mechanical Engineering, Lovely Professional University, Phagwara, India
[b] Department of Mechanical Engineering, Dr. B.R. Ambedkar National Institute of Technology, Jalandhar, India
[c] School of Mechanical, Materials & Energy Engineering (SMMEE), Indian Institute of Technology, Ropar, India

ARTICLE INFO

Article history:
Received 31 January 2015
Accepted 11 March 2015
Available online 23 April 2015

Keywords:
Carbon nanotube
Damping
Mechanical properties
Molecular dynamics
Polycarbonate
Thermal conductivity

ABSTRACT

The present study aims at examining the mechanical properties of multi-walled carbon nanotubes–polycarbonate composites (MWCNT–PC), through a molecular dynamics (MD) simulation. Composites of MWCNT–PC were modeled using Materials Studio 5.5 software. Multiwall carbon nanotubes (MWCNTs) compositions in polycarbonate (PC) were varied by weight from 0.5% to 10% and also by volume from 2% to 16%. Forcite module in Materials Studio was used for finding mechanical properties. A marked increase in the elastic modulus (up to 89%) has been observed, even with the addition of a small quantity (up to 2 weight %) of MWCNTs. Also, upon addition of about 2 volume % of MWCNTs, the elastic modulus increases by almost 10%. The increase in mechanical properties is found to supplement earlier experimental investigations of these composites using nano-indentation techniques. Better load transfer property of MWCNTs, larger surface area and interaction between reinforcement with base matrix are the suggested reasons for this increase in mechanical properties.

1. Introduction

Carbon nanotubes are excellent reinforcements for polymers because of their unique mechanical properties and large surface area per unit volume. Experiments and calculations show that nanotubes have a modulus equal to or greater than the best graphite fibers, and strengths at least an order of magnitude higher than typical graphite fibers. For example, the measurement of the tensile properties of individual multi-walled carbon nanotubes (MWCNTs) gave values of 11–63 GPa for the tensile strength and 270–950 GPa for Young's modulus, as obtained by Yu et al. [1]. For comparison, the modulus and strength of graphite fibers are 300–800 and 5 GPa, respectively. In addition to their outstanding mechanical properties, the surface area per unit volume of nanotubes is much larger than that of embedded graphite fibers. For example, 30-nm-diameter nanotubes have 150 times more surface area than 5-μm-diameter fibers for the same filler volume fraction, such that the nanotube/matrix interfacial area is much larger than that in traditional fiber-reinforced composites. The

* Corresponding author. Tel.: +91 8146871758.
E-mail address: sumit_sharma1772@yahoo.com (S. Sharma).
[1] Assistant Professor.
[2] Professor.
[3] Associate Professor.

http://dx.doi.org/10.1016/j.crme.2015.03.002
1631-0721/

unusual mechanical strength of the carbon nanotubes has motivated scientists to fabricate and modify other useful materials which are cheaply available in bulk form, by combining them as composites with carbon nanotubes. Polycarbonate (PC) is a lightweight polymer that is available in bulk form and is widely used for several engineering applications due to its moldability. For taking advantage of the useful properties of polymers in combination with unique structural properties of carbon nanotubes, multi-walled carbon nanotubes–polymer composites have been researched and fabricated over the past few years. In order to exploit the usefulness of these composites for specific mechanical engineering applications, their static and dynamic mechanical properties need to be evaluated. Among the static properties, the elastic modulus of the specimen is very important.

A lot of work has been published related to tensile testing of MWCNT–PC composites. These tests have evidenced that minor compositions (up to 2 wt. %) of MWCNT in PC enhance the modulus and tensile strength from 10% to even 70%. Choi et al. [2] used styrene and acrylo-nitrile (SAN) grafted MWCNTs with PC instead of pristine MWCNTs and observed that when SAN-grafted MWCNTs (1 wt. %) were used with PC, both tensile strength and modulus increased by nearly 5% and 10%, respectively, in comparison to pristine MWCNT–PC composites. Liu et al. [3] observed that at 3 wt. % MWCNTs in a PC, the composites exhibited a nearly 40% higher tensile strength in comparison to pure PC. However, for a 5 wt. % MWCNT composition, the strength reduced drastically. There are also contrary results obtained by Olek et al. [4], who reported no improvement in the presence of MWCNTs in the polymer poly-methyl-methacrylate (PMMA) for any static mechanical property. Even with a compositional change from 1% to 5% of MWCNTs, the elastic modulus remained almost the same as that of pure PMMA. However, if the MWCNTs were coated with silica, the composite showed remarkable results upon nano-indentation. With only 4% MWCNT–silica in PMMA, the modulus measured is about three times that of pure PMMA. Reinforcement on poly-vinyl alcohol (PVA) and PMMA with few-layer graphene (FG) was also tested using a nano-indenter by Das et al. [5].

Low compositions of FG (0.6%) in PVA made the modulus increase by about 20%. Vivekchand et al. [6] have explained the use of inorganic nanowires (NW) as reinforcement in PVA to be as efficient as MWCNTs. The elastic modulus increased by almost two times upon reinforcement by 0.8% (in volume) of inorganic NW. However, MWCNTs have a very smooth surface; making the strength imparted by reinforcing with MWCNTs lesser than with NW. Kim et al. [7] used a compatibilizer as two poly-g-polycapro-lactones (P3HT-g-PCLs) with bisphenol-A-PC-MWCNT composite. When a PC-MWCNT composite was combined with P3HT-g-PCL, then there was an increase of nearly 22% in the Young modulus and 30% in the tensile strength in comparison to pure PC. For small concentrations (0.1–0.5 wt. %) of MWCNTs, this increase was found to be consistent. However, when the MWCNTs concentration was further increased to 1 wt. %, then both Young's modulus and tensile strength were considerably reduced.

Eitan et al. [8] used bisphenol-A-PC with MWCNTs as composites for mechanical characterization. Tensile tests were performed using a Universal Testing Machine and it was found that for composites with surface-modified MWCNTs (5 wt. %), the modulus improved by 95% in comparison to pure PC. Even for composites using pristine MWCNTs (5 wt. %), the modulus rise was nearly 70% in comparison to pure PC. Ayatollahi et al. [9] have used epoxy-MWCNT composite under shear and bending load using a Santan Universal Testing Machine. They have also found that there is a gradual increase in elastic modulus and tensile strength as MWCNT composition increased in epoxy. Compositions of 0.1%, 0.5% and 1.0% MWCNTs in epoxy were fabricated and, as the composition of MWCNTs increased, both elastic modulus and tensile strength increased by 10%. Montazeri et al. [10] used a Hounsfield machine and also evaluated the viscoelastic behavior of epoxy-MWCNT composite. They reported that with further increase in MWCNT composition of 2%, the elastic modulus increased by about 20% as compared to pure epoxy samples.

Computational studies complement experiment by providing easy manipulation, analysis and insights into the molecular level. The extent to which mechanical reinforcement can be achieved depends on several factors, including uniformity of dispersion, degree of alignment of CNTs, and the strength of polymer–CNT interfacial bonding. Since it is difficult to control and measure many of these properties experimentally, computational modeling can provide some crucial insights. For this reason, theoretical and computational methods have been widely applied to study polymer/CNT composites.

Due to the difficulties in the experimental characterization of nanotubes, computer simulation has been regarded as a powerful tool for modeling the properties of nanotubes. Among the available modeling techniques, molecular dynamics simulation has been used most extensively. First-principles methods are able to generate reasonably accurate data of structures and energies relevant to polymer nanocomposite systems, but they can only be used to study small systems over short times due to their computational expense. In contrast, molecular simulation methods such as molecular mechanics (MM) and molecular dynamics (MD), which are based on analytic force fields, are computationally cheaper compared to first-principles methods. They can therefore be used to study larger molecular systems for longer times. As described below, MD can also be used to obtain macroscopic properties such as the Young modulus.

The present study was undertaken to investigate changes in the static mechanical properties under the influence of varying compositions (per weight and per volume) of pristine MWCNTs in PC by employing the MD technique without any additional component or any surface modification in the composite. The elastic modulus has been studied to supplement the experimental investigations on these composites made by Kumar et al. [11]. They prepared composites of MWCNT–PC by a two-step method of solution blending, followed by compression molding. Multiwall carbon nanotubes (MWCNTs) compositions in polycarbonate (PC) were varied by weight from 0.5% to 10%. Nano-indentation techniques were used to evaluate mechanical properties like elastic modulus and hardness. A marked increase in the elastic modulus (up to 95%) was observed with the addition of small quantities (up to 2 wt. %) of MWCNTs.

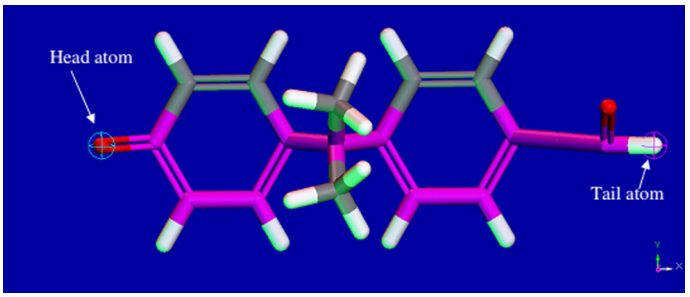

Fig. 1. (Color online.) A carbonate monomer.

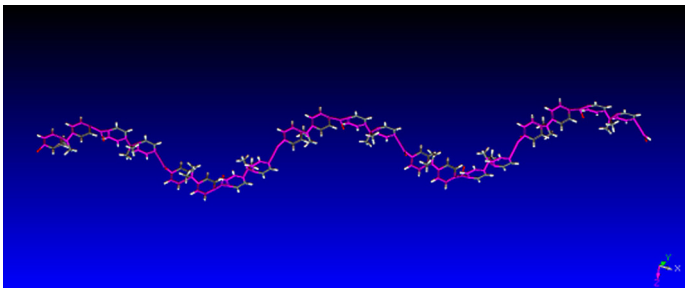

Fig. 2. (Color online.) Polycarbonate chain containing ten repeat units of carbonate.

These properties will help us in the mechanical characterization of PC-based composites and in the evaluation of the usefulness of MWCNTs as reinforcement from the point of view of applications.

2. Simulation strategy

Our MD simulations were performed by Materials studio 5.5. We used Condensed-phase Optimized Molecular Potentials for Atomistic Simulation Studies (COMPASS) force field, which is implanted in Materials studio 5.5. COMPASS is the first force field that has been parameterized and validated using condensed phase properties in addition to empirical data for molecules in isolation. Consequently, this force field enables accurate and simultaneous prediction of structural, conformational, vibrational, and thermo-physical properties for a broad range of molecules in isolation and in condensed phases. The COMPASS force field consists of terms for bonds (b), angles (θ), dihedrals (φ), out-of-plane angles (χ) as well as cross-terms, and two non-bonded functions, a Coulombic function for electrostatic interactions and a 9–6 Lennard–Jones potential for van der Waals interactions.

$$E_{\text{total}} = E_b + E_\theta + E_\varphi + E_\chi + E_{b,b'} + E_{b,\theta} + E_{b,\varphi} + E_{\theta,\varphi} + E_{\theta,\theta'} + E_{\theta,\theta',\varphi} + E_q + E_{\text{vdW}} \tag{1}$$

where

E_b = energy due to bond stretching,
E_θ = energy due to bond bending,
E_φ = energy due to bond torsion,
E_χ = energy due to out of plane inversion,
E_q = electrostatic energy,
E_{vdW} = van der Waals energy and
$E_{b,b'}$, $E_{\theta,\theta'}$, $E_{b,\theta}$, $E_{b,\varphi}$, $E_{\theta,\varphi}$, $E_{\theta,\theta',\varphi}$ = cross terms representing the energy due to the interaction between bond stretch–bond stretch, bond bend–bond bend, bond stretch–bond bend, bond stretch–bond torsion, bond bend–bond torsion and bond bend–bond bend–bond torsion, respectively.

All the simulations were done in the constant temperature and constant volume canonical ensemble (NVT). The equations of motions were integrated using the Verlet algorithm with an integration time step of 1 fs and the temperature was controlled by Andersen's thermostat. The total simulation time for the dynamics run was 50 ps, with a time step of 1 fs. After the completion of dynamics run, the structure obtained was first subjected to geometry optimization using a conjugate gradient algorithm and then a stain of 0.005 was applied to obtain the elastic moduli. Periodic boundary conditions were used in all simulations.

Fig. 1 and Fig. 2 show, respectively, the chemical structure of the investigated carbonate and PC polymer. Firstly, a repeat unit was built using the 'Build' tool in Materials studio 5.5. Then, using the same tool, the PC structure was obtained by

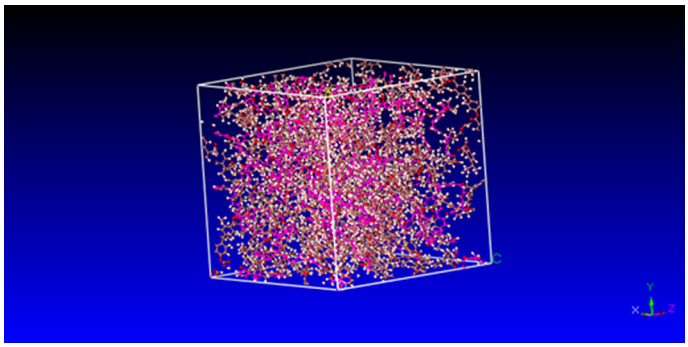

Fig. 3. (Color online.) Simulation cell of pure PC containing 17,728 atoms.

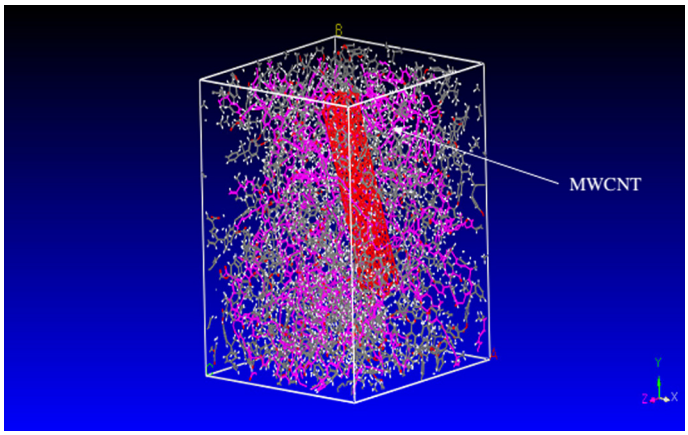

Fig. 4. (Color online.) Simulation cell of MWCNT (0.75% by weight) reinforced PC containing 20,273 atoms.

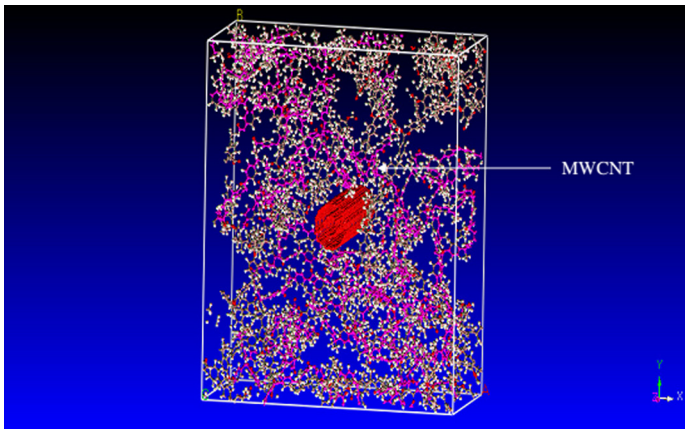

Fig. 5. (Color online.) Simulation cell of MWCNT (2% by volume) reinforced PC containing 20,173 atoms.

polymerizing the carbonate repeat unit and taking the chain length as ten. Fig. 3 shows a simulation cell of pure PC. The density of the cell was 1.5 g/cm^3 and the cell dimensions were taken as: $49.3 \times 49.3 \times 49.3$ Å^3. The molecular model of MWCNT/PC composites with different dimensions was built with the use of the "Amorphous cell" module. Firstly, a MWCNT of length 41.81 Å was constructed using the "Build nanostructure" dialog box in Materials Studio. The configuration of the inner and outer nanotubes was taken as (3,3) and (6,6) respectively. This tube was then inserted in a simulation cell of the required dimensions. Lastly, PC was packed around the MWCNT using the "Packing" feature available in Amorphous Cell. In this study, simulations were performed in two ways. In the first approach, MWCNTs were packed in PC by weight and in the second approach, packing was done by volume. Fig. 4 and Fig. 5 show, respectively, the structures obtained after packing by weight and by volume. Similar to Figs. 4–5, a number of simulation cells were created in the software, and mechanical properties were obtained.

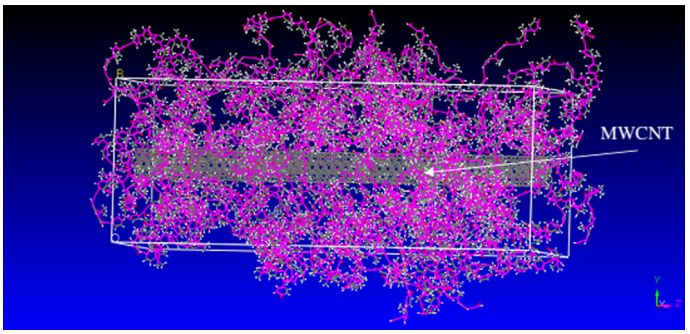

Fig. 6. (Color online.) Simulation cell of MWCNT ($V_f = 0.04$, $l/d = 30$) reinforced PC composite containing 20,798 atoms.

A number of simulations were also performed for a fixed MWCNT volume fraction and by varying the aspect ratio. The aspect ratio of MWCNTs was varied from $l/d = 5$ to $l/d = 100$. Fig. 6 shows one of the simulation cells of an MWCNT-reinforced PC composite with $V_f = 0.04$ and $l/d = 30$. A similar approach was adopted while modeling zigzag and chiral MWCNT-reinforced PC composites.

3. Thermal conductivity

With the dimensions of electronic and mechanical devices approaching the nanometer scale, efficient heat removal is of crucial importance to both performance and function. While a basic understanding of heat transport in dielectrics has already been achieved, many important issues remain unresolved. The interpretation of experimental results remains difficult because typically the contributions of individual defects cannot be deconvoluted. MD simulations are ideal for addressing such issues since they can be used to study individual microstructural elements, thereby identifying the most important issues for thermal conductivity in polycrystalline materials. For example, by elucidating the correlation between grain-boundary structure and thermal-transport properties, one may hope to eventually design materials with tailored thermal properties. However, prior to a systematic study of interfacial effects, it is necessary to firmly establish suitable computational methods. The thermal conductivity relates the heat current to the temperature gradient via Fourier's law as:

$$J_\mu = -\sum_\nu \kappa_{\mu\nu} \frac{\partial T}{\partial x_\nu} \tag{2}$$

where J_μ is a component of the thermal current, $\kappa_{\mu\nu}$ is an element of the thermal conductivity tensor, and $\partial T/\partial x_\nu$ is the gradient of the temperature T. Experimentally, κ is typically obtained by measuring the temperature gradient that results from the application of a heat current.

In MD simulations, thermal conductivity can be computed either using non-equilibrium MD (NEMD) or equilibrium MD (EMD). The two most commonly applied methods for computing thermal conductivity are the "direct method" and the Green–Kubo method. The direct method is an NEMD method that relies on imposing a temperature gradient across the simulation cell and is therefore analogous to the experimental situation. By contrast, the Green–Kubo approach is an EMD method that uses current fluctuations to compute the thermal conductivity via the fluctuation–dissipation theorem. Schelling et al. [12] studied and compared the features of each method. They pointed out that NEMD might contain non-linear effects due to the application of the required temperature gradient. They also noted that while both EMD and NEMD approaches exhibit finite size effects, these effects are much more severe in NEMD due to the presence of interfaces at the heat source and sink. Furthermore, EMD facilitates thermal conductivity prediction in all directions using one simulation, whereas NEMD requires the use of a thermal gradient and therefore only enables the calculation of thermal conductivity in one direction. Therefore, EMD is particularly useful for geometries where periodic boundary conditions can be applied. However, the basis of EMD is the fluctuation–dissipation theorem, while NEMD's basis in Fourier's Law of conduction makes NEMD analogous to experimental measurements. Furthermore, EMD has been often computationally more expensive and the results are more sensitive to simulation parameters.

In EMD, the system is set to the desired temperature, and then a constant energy scheme is used with the well-known Green [13] and Kubo [14] relations to calculate the thermal conductivity tensor. MD simulations may be applied to different statistical ensembles, namely canonical (NVT), grand-canonical (μPT), and micro-canonical (NVE). It is worth noting that their derivations have been done in different ensembles: the former in micro-canonical and the latter in grand-canonical. Lepri et al. [15] resolved this discrepancy by noting that if the micro-canonical ensemble is used, then the thermal conductivity might diverge non trivially unless the velocity of the center of mass of the system is set to zero or alternatively some terms are subtracted from the calculated heat flux vectors. However, the canonical ensemble can also be used with the Green–Kubo formula to predict the thermal conductivity by applying additional thermal forces to all the atoms. Dynamic properties such as thermal conductivity are calculated in EMD based on the fluctuation dissipation and linear response theorem. This method applies the fact that the heat flow in a system of particles in the equilibrium state fluctuates around

zero. The heat flux vectors and their correlations are computed throughout the simulations. The time needed for Heat Auto-Correlation Functions (HACF) to decay to zero is then used through the Green–Kubo relation to predict the thermal conductivity.

NEMD simulations provide a means to calculate thermal conductivity in a way analogous to the experimental measurements either by imposing a thermal gradient into the system of particles or by introducing a heat flow.

In the reverse non-equilibrium MD (RNEMD) method, the energy exchange is carried out by exchanging the kinetic energy of two particles: the hottest particle in the cold layer and the coldest particle in the hot layer. The energy ΔE is therefore variable and needs averaging over many exchanges. In the method of Jund [16], the energy ΔE is fixed, and involves all particles in the hot and cold layers. Both methods conserve total linear momentum and energy of the system. The imposed flux method of Jund [16] also conserves the total linear momentum of the hot and cold layer, i.e. no momentum is exchanged.

In this study, the imposed flux method was used to find thermal conductivity. The number of layers in which the direction of the flux is divided was fixed at 40. Increasing the number of layers can increase the accuracy of the gradients, but too many layers will lead to large fluctuations in the layer temperatures. Two types of exchange method were used in the study. The first is "VARIABLE", which exchanges a variable energy between one object in the hot layer and one in the cold layer. "FIXED" exchanges a constant energy between all hot objects in the hot layer and all objects in the cold layer. The amount of energy to exchange in each step when using the "FIXED" exchange type was taken as 1 kcal/mol. The flux was determined by the ratio of exchange energy and number of steps. The number of exchanges during the equilibration stage was taken as 500. During the equilibration stage, a thermostat (NVT) acts on the system. The number of exchanges during the production stage was equal to 1000. The production stage was carried out at constant energy (NVE). A time step of 1 fs was used in the simulation. The number of time steps in between two exchanges was fixed at 100. Decreasing the number of steps leads to higher fluxes and increases the temperature gradient. Too small values were avoided as these introduce nonlinear effects and may impact performance.

To find thermal conductivity, MD simulations were performed with MWCNT volume fraction varying from $V_f = 0$–0.16 and the aspect ratio was kept fixed at $l/d = 10$. Also, simulations were performed with varying the aspect ratio (l/d) of MWCNT and the fixed volume fraction $V_f = 0.04$. Thermal conductivity results obtained using MD simulations were compared with other models such as series model, parallel model, Maxwell–Garnett model, Lewis–Nielsen model, and Hamilton–Crosser model. Comparison of MD results for thermal conductivity was made with Deng's model. A brief introduction to these models will be given in the next section.

4. Models to calculate thermal conductivity

Many theoretical and semi-theoretical models are available to represent the effective thermal conductivity of conventional polymer composites in which large-size fillers have been dispersed in a polymer matrix. Simple models such as the series model give the lower bound, whereas the parallel model (rule of mixture) gives the upper bound of the thermal conductivity of a nanocomposite. As might be expected, experimental observations suggest that real values for nanocomposites fall somewhere in between these two limits.

4.1. Parallel and series models

Both the series model and the parallel model assume that each phase contribute independently to the overall thermal resistance and conductance, respectively, and assume a perfect interface between any two phases in contact. The series model applies readily to the thermal conductivity of a laminated composite along the stacking direction. However, it typically gives an underestimation of thermal conductivity due to the presumably complete localization of the contribution from the fibers embedded in the matrix, neglecting the interaction among the fillers. Therefore, the series model gives the lower bound for the thermal conductivity of composites. The series model of thermal conductivity is given by:

$$k = (k_m \times k_f)/\big(k_f \times (1 - v_f) + k_m \times v_f\big) \tag{3}$$

where,

k = thermal conductivity of composite
k_m = thermal conductivity of polycarbonate matrix = 0.15 W/m/K
k_f = thermal conductivity of armchair MWCNT = 30 W/m/K
v_f = MWCNT volume fraction

In comparison, the parallel model predicts the thermal conductivity of conventional continuous fiber-reinforced composites along the fiber alignment direction. The rule of mixture implicitly assumes perfect contact between fibers. However, it gives a large overestimation of thermal conductivity and gives an upper bound for thermal conductivity of composites. It is worth pointing out that thermal conductivity measurement results of composites should always fall between the predictions of the series model (lower bound) and the parallel model (upper bound), except for the cases where interfacial phonon scattering in nano-laminates can yield even lower thermal conductivity than the lower bound by the series model.

For the parallel model, thermal conductivity is given as

$$k = (1 - v_f) \times k_m + v_f \times k_f \tag{4}$$

where the symbols have the same meaning as previously described in the series model.

4.2. Maxwell–Garnett model

The problem of determining the effective transport properties of multiphase materials dates back to Maxwell. Based on the continuity of potential and electric current at the interface, and on the assumption that the interactions among the fibers are negligible, which means that the disseminated fibers are located far enough from each other, Maxwell derived an analytical formula for the effective specific resistance (K) of "a compound medium consisting of a substance of specific resistance K_2, in which are disseminated small spheres of specific resistance K_1, the ratio of the volume of all the small spheres to that of the whole, being p." When transformed to the thermal conductivity (k) discussed here, the model gives:

$$k = k_m + \left[3 \times v_f \times (k_f - k_m)/(2 \times k_m + k_f - v_f \times (k_f - k_m)\right] \tag{5}$$

Eq. (5) gives satisfactory results for composites with: (i) very low v_f, (ii) good dispersion, and (iii) no interfacial thermal resistance. It is also referred to as Maxwell–Garnett (MG) equation.

4.3. Lewis–Nielsen model

In this model, conductivity becomes the analog of stiffness or the elastic shear modulus, and the disturbance of the flux field becomes analogous to the disturbance of the stress field by the dispersed filler. Starting from the Halpin–Tsai [17] equations, which are widely used in micro-mechanics, Nielsen applied a modified equation, the Nielsen–Lewis equation, to the modeling of thermal conductivity:

$$k = k_m \times \left[(1 + A \times B \times v_f)/(1 - B \times \psi \times v_f)\right] \tag{6}$$

where

$$A = k_E - 1$$

k_E is the generalized Einstein coefficient, and depends primarily upon the shape of the fillers and how they are oriented with respect to the direction of the heat flow. In our case, A = 2 $l/d = 10$,

$$B = \left[(k_f/k_m) - 1\right]/\left[(k_f/k_m) + A\right]$$

$$\psi = 1 + 1.775 \times v_f$$

k_m = thermal conductivity of polycarbonate matrix = 0.15 W/m/K
k_f = thermal conductivity of armchair MWCNT = 30 W/m/K
v_f = MWCNT volume fraction.

Although Nielsen's model is a semi-empirical model, significant improvements in the model should be appreciated. The shape effect and to some extent the orientation effect are both taken into account. Reduced filler loading (ψ) accounts for the maximum packing density of the fillers with a specific shape and size distribution, and is unique to this model. In comparison, most of the theoretical equations assume uniform changes of filler loading up to the point where the dispersed phase makes up the complete system, which is not realistic. The Nielsen–Lewis equation gives a higher prediction than the Maxwell–Garnett equation, mainly because of the reduced filler loading. However, we should note that the model gives too high a prediction at high filler loading. In addition, interfacial thermal resistance is not considered in this model.

4.4. Hamilton–Crosser model

The Hamilton and Crosser model [18] is an extension of Maxwell's theory accounting for the non-sphericity of fillers through the use of a shape factor, n, defined as $n = 3/\psi$, with ψ being the particle sphericity. The sphericity ($\psi = A_e/A$) of a particle is defined as the ratio of the surface area (A_e) of the equivalent sphere having the same volume to the actual surface area (A) of the non-spherical fiber. The effective thermal conductivity of the Hamilton and Crosser model is given by:

$$k = k_m \left[\frac{k_f + 5k_m - 5v_f \times (k_m - k_f)}{k_f + 5k_m + v_f \times (k_m - k_f)}\right] \tag{7}$$

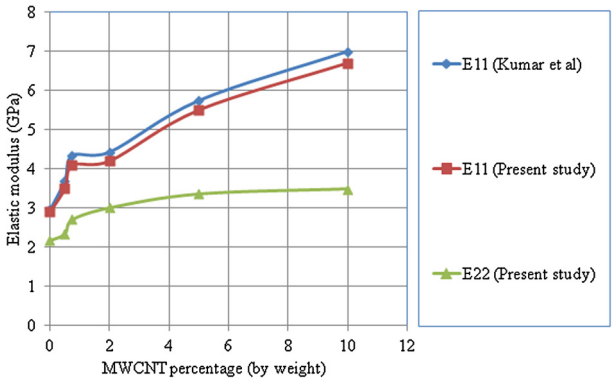

Fig. 7. (Color online.) Variation of Young's modulus, E_{11} and E_{22}, with the percentage of MWCNT (by weight) in PC.

where

k_m = thermal conductivity of polycarbonate matrix = 0.15 W/m/K,
k_f = thermal conductivity of armchair MWCNT = 30 W/m/K,
v_f = MWCNT volume fraction.

Since neither interfacial resistance nor fiber–fiber interaction was taken into account, the fiber size was found to have no influence on the effective thermal conductivity of the composite in this model.

4.5. Deng model

For estimating the mechanical and thermal properties of inclusion-in-matrix composites, even for those with high concentrated inclusions, so that the interactions among the inclusions must be considered, some mature methods have been established within the framework of micro-mechanics. For CNT composites with low loadings of randomly oriented straight CNTs of average length L and diameter d, an analytical estimate for the effective thermal conductivities, k_e, of the CNT composites can be given in the following form:

$$\frac{k_e}{k_m} = 1 + \frac{\frac{v_f}{3}}{\frac{k_m}{k_f} + H} \tag{8}$$

where

k_e = equivalent thermal conductivity of the composite,
k_m = thermal conductivity of polycarbonate matrix = 0.15 W/m/K,
k_f = thermal conductivity of armchair MWCNT = 30 W/m/K,
v_f = MWCNT volume fraction,

$$H = \frac{1}{p^2-1}\left[\frac{p}{\sqrt{p^2-1}}\ln\left(p+\sqrt{p^2-1}\right) - 1\right],$$
$$p = l/d.$$

5. Results and discussion

This section has been divided into two parts. In Section 5.1, we have discussed the results obtained for elastic moduli. In Section 5.2, we have explained the damping results and in Section 5.3, we have examined the results of thermal conductivity.

5.1. Elastic moduli

Fig. 7 shows the variation of Young's modulus E_{11} and E_{22}, with the percentage of MWCNT (by weight) in PC. Both moduli show an increasing trend with an increase in the weight percentage of MWCNT. However, the increase in transverse modulus, E_{22}, is too low in comparison to that of E_{11}. This confirms the fact that MWCNT–PC composites when loaded in transverse direction behave poorly. Moreover, it can be inferred from Table 1 and Fig. 7 that when increasing the MWCNT weight percentage by 0–5%, the increase in moduli is greater than when the MWCNT weight percentage increases by 5–10%. The improvement in mechanical properties was found for minor compositions of MWCNTs in PC and they further increased as the composition of MWCNTs was increased. However, beyond a certain limit of composition, this pattern was not followed. It has been argued that proper dispersion at lower compositions, stronger π–π interaction between MWCNTs and

Table 1
Percentage increase in moduli when increasing the weight percent of MWCNT.

MWCNT (weight %)	Percentage increase in longitudinal modulus (E_{11})	Percentage increase in transverse modulus (E_{22})
0–5	89.65	54.13
5–10	21.81	3.87

Table 2
Percentage difference between Kumar et al. [11] and present study for the longitudinal modulus (E_{11}).

MWCNT (weight %)	Percentage difference
0	2.03
0.50	5.40
0.75	5.75
2	5.20
5	4.18
10	4.14

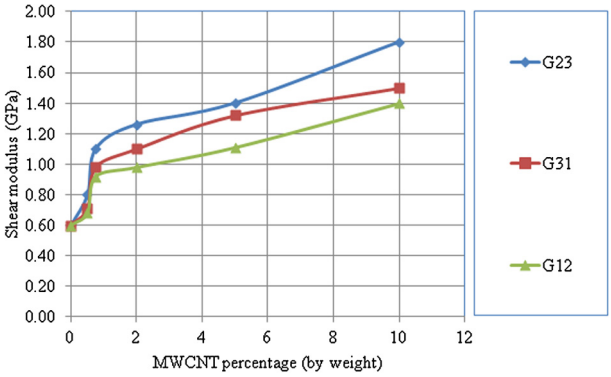

Fig. 8. (Color online.) Variation of the shear modulus with the percentage of MWCNT (by weight) in PC.

Table 3
Percentage increase in shear moduli when increasing the MWCNT weight percentage.

MWCNT range (weight %)	Increase in shear moduli (in %)		
	G_{23}	G_{31}	G_{12}
0–2	110	83.33	63.33
2–10	42.85	36.36	35.45

base matrix, combination of large aspect ratio and high surface-to-volume ratio of MWCNTs and improved load transfer capability of MWCNTs assisted in the improvement of the properties, but for higher compositions, aggregates of MWCNTs were formed and the curvy and slippery nature of MWCNTs did not assist in further improvement of the mechanical properties.

From Table 2 and Fig. 7, it can be inferred that the results of our study supplement the experimental study conducted by Kumar et al. for the same material. As can be observed from Table 2, MD simulation results from this study are close to the experimental results. Fig. 8 shows the variation of shear moduli, G_{23}, G_{31} and G_{12} with MWCNT weight percentage. Comparing Fig. 7 and Fig. 8, it can be concluded that MWCNT-reinforced PC composites are weak when loaded in shear in comparison to when loaded in tension. Though the shear moduli increase with the MWCNT weight percentage, the rise is much lesser when compared with the rise in longitudinal modulus E_{11}. Table 3 shows that initially, when increasing the MWCNT weight percent from 0–2, the rise in all the shear moduli is greater in comparison to the increase in shear moduli when MWCNT weight percent increases by 2 to 10. This is due to the curvy and slippery nature of MWCNTs.

Fig. 9 shows the variation of Young's moduli, E_{11} and E_{22}, with the percentage of MWCNT (by volume) in PC. It shows that the longitudinal modulus (E_{11}) increases when increasing the MWCNT volume fraction. The percent increase in E_{11} when increasing the MWCNT volume fraction is shown in Table 4. From Fig. 9 and Table 4, it can be observed that E_{11} increases sharply till the MWCNT volume fraction is 2%. Thereafter, the rise is minimal due to the aggregation of MWCNTs and the curvy and slippery nature of MWCNTs does not assist in further improvement of the mechanical properties. Fig. 9 also shows that the increase in the transverse modulus (E_{22}) is negligible in comparison to the rise in E_{11}. This is due to the fact that the fibers are aligned in the longitudinal direction. As the percentage of MWCNT (by volume) in PC increases,

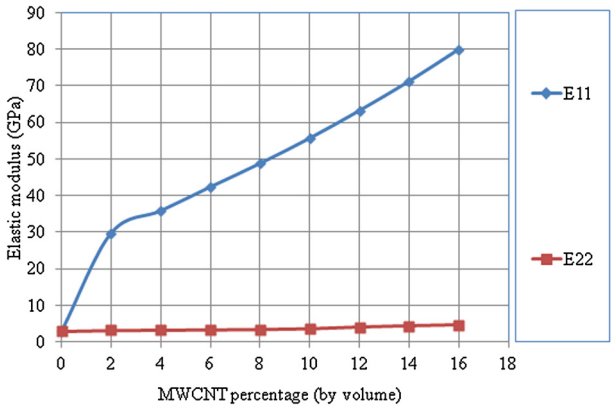

Fig. 9. (Color online.) Variation of Young's modulus, E_{11} and E_{22}, with the percentage of armchair MWCNT (by volume) in PC.

Table 4
Percentage variation in longitudinal modulus (E_{11}) when increasing the MWCNT volume fraction.

MWCNT (volume %)	Percentage difference in longitudinal modulus (E_{11}) w.r.t. previous value	Percentage increase in E_{11}	
0	–	from $V_f = 0$ to $V_f = 6\%$	from $V_f = 6$ to $V_f = 16\%$
2	925.86		
4	20.50		
6	18.27		
8	15.09	1362.07	88.63
10	14.16		
12	13.51		
14	12.69		
16	12.22		

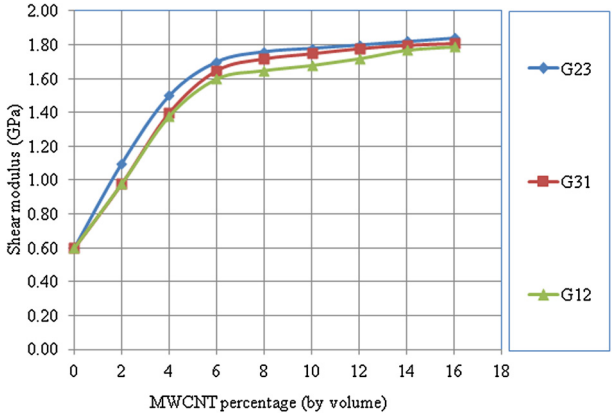

Fig. 10. (Color online.) Variation of the shear modulus with the percentage of armchair MWCNT (by volume) in PC.

the volume of the fibers is increasing. Since MWCNTs have a high modulus in the longitudinal direction, the composite has improved properties in the said direction. In the transverse direction, the properties of the composite are matrix dominated and hence lower values of E_{22} are observed.

Fig. 10 shows the variation of shear moduli when increasing the MWCNT volume fraction. When increasing the MWCNT volume fraction by 0–0.06%, the percent increase in transverse shear modulus G_{23} is approximately 183%, whereas the percent increase reduces to merely 10% when the MWCNT volume fraction increases by 0.06–0.16. Also, the rise in all the shear moduli is negligible in comparison to the rise in E_{11}. This is again due to the fact that in every shear mode, the properties of the composite are matrix dominated and hence lower values of all shear moduli are observed. Table 5 shows the percentage increase in shear moduli when increasing the MWCNT volume fraction.

Fig. 11 shows the variation of Young's modulus (E_{11}) with the percentage of MWCNT (by volume) in PC, for different configurations of MWCNT. All the simulations were performed with MWCNT aspect ratio ($l/d = 10$). The carbon atoms in a CNT are in sp^2 configurations and connected to one another by three strong σ bonds. Due to the geometric orientation of the carbon–carbon bonds relative to the nanotube axis, armchair MWCNT-reinforced PC composites exhibit high tensile

Table 5
Percentage increase in shear moduli when increasing the MWCNT volume fraction.

MWCNT range (volume %)	Increase in shear moduli (in %)		
	G_{23}	G_{31}	G_{12}
0–6	183.33	175	166.66
6–16	9.73	9.69	9.15

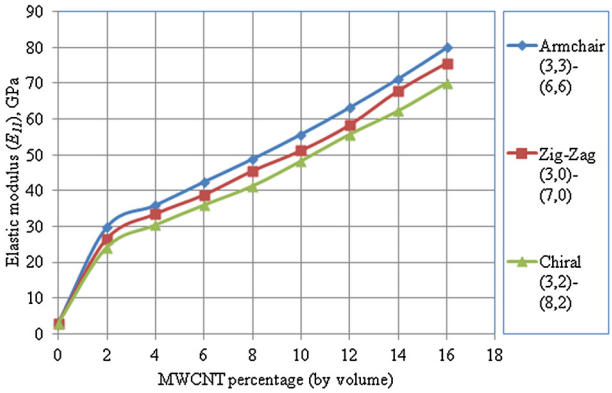

Fig. 11. (Color online.) Variation of Young's modulus (E_{11}) with the percentage of MWCNT (by volume) in PC, for different configurations of MWCNT.

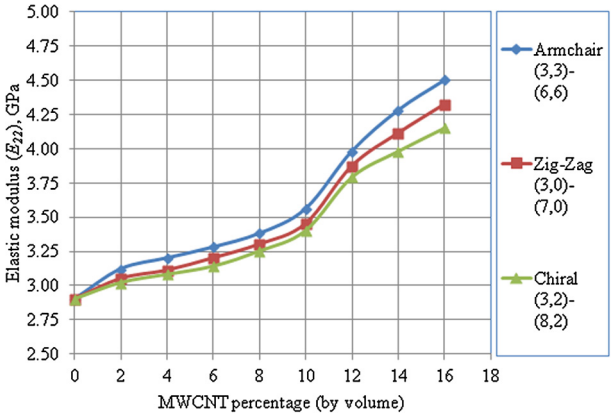

Fig. 12. (Color online.) Variation of Young's modulus (E_{22}) with the percentage of MWCNT (by volume) in PC, for different configurations of MWCNT.

Table 6
Percentage increase in elastic moduli when increasing MWCNT volume fraction.

MWCNT range (volume %)	Increase in moduli (in %)					
	Armchair		Zigzag		Chiral	
	E_{11}	E_{22}	E_{11}	E_{22}	E_{11}	E_{22}
0–6	1362.07	13.10	1234.82	10.35	1137.58	8.27
6–16	98.63	37.20	95.17	35.00	95.16	32.16

strength and Young's moduli values compared to the zigzag MWCNT-reinforced PC composites. Chiral MWCNT-reinforced PC composites have lower elastic moduli because of the curved nature of all C=C sp^2 bonds.

Fig. 12 shows the variation of Young's modulus (E_{22}) with the percentage of MWCNT (by volume) in PC, for different configurations of the MWCNT. Comparing Fig. 11 and Fig. 12, it can be observed that the increase in E_{22} is smaller than that of E_{11}. Table 6 shows the percentage increase in elastic moduli upon increasing the MWCNT volume fraction. From Fig. 11 and Table 6, it can be inferred that initially, when increasing the MWCNT volume fraction by 0–6%, the rise in the elastic modulus E_{11} is faster when compared with the rise in modulus later on. From Figs. 11–12 and Table 6, it can be concluded that the percentage rise in moduli is greatest for armchair MWCNT-reinforced PC composites.

Fig. 13 shows the variation of the shear modulus (G_{23}) with the percentage of MWCNT (by volume) in PC, for different configurations of MWCNT. It can be observed that the increase in shear modulus is the greatest for armchair MWCNT-

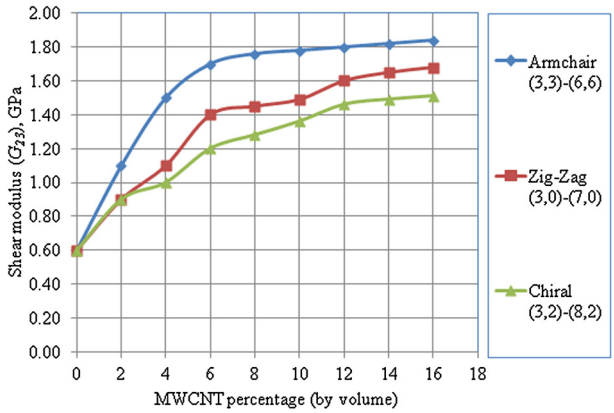

Fig. 13. (Color online.) Variation of the shear modulus (G_{23}) with the percentage of MWCNT (by volume) in PC, for different configurations of MWCNT.

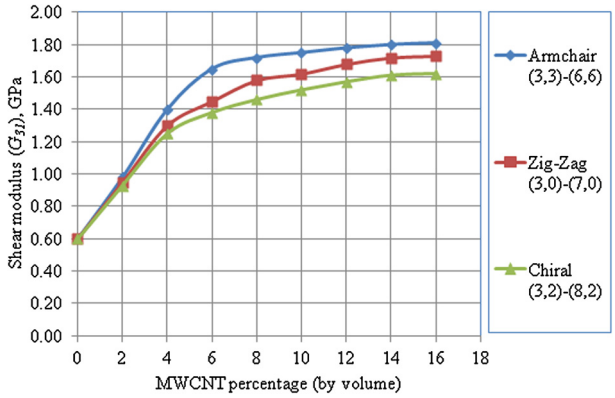

Fig. 14. (Color online.) Variation of the shear modulus (G_{31}) with the percentage of MWCNT (by volume) in PC, for different configurations of MWCNT.

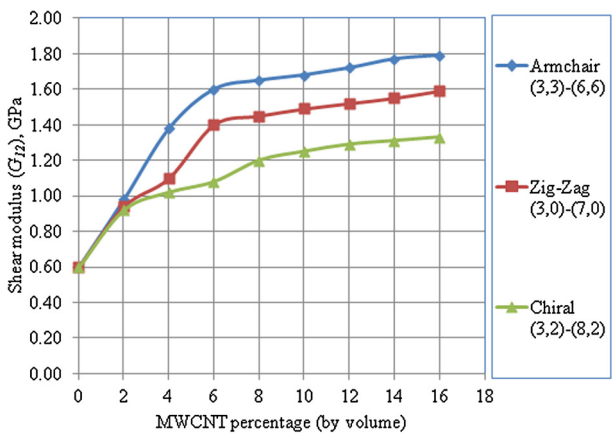

Fig. 15. (Color online.) Variation of the shear modulus (G_{12}) with the percentage of MWCNT (by volume) in PC, for different configurations of MWCNT.

reinforced PC composites. Also, the values are considerably smaller in comparison to the values of the longitudinal elastic modulus.

Fig. 14 shows the variation of the shear modulus (G_{31}) with the percentage of MWCNT (by volume) in PC, for different configurations of MWCNT. The values of G_{31} are smaller in comparison to the values of G_{23}. Fig. 15 shows the variation of the shear modulus (G_{12}) with the percentage of MWCNT (by volume) in PC, for different configurations of MWCNT. The variation is similar to that observed for G_{31}.

Table 7 shows the percentage increase in shear moduli with an increase in the MWCNT volume fraction. It shows that the percentage increase in modulus is the greatest for armchair MWCNT-reinforced PC composites. Initially, the increase in all the shear moduli is faster, when the MWCNT volume fraction increases by 0–6%, in comparison to the increase

Table 7
Percentage increase in shear moduli when increasing the MWCNT volume fraction.

MWCNT range (volume %)	Increase in moduli (in %)								
	Armchair			Zigzag			Chiral		
	G_{23}	G_{31}	G_{12}	G_{23}	G_{31}	G_{12}	G_{23}	G_{31}	G_{12}
0–6	183.33	175.00	166.66	143.33	141.66	133.33	132.45	130.00	80.00
6–16	28.23	19.70	13.87	20.00	19.31	13.57	15.83	13.40	13.14

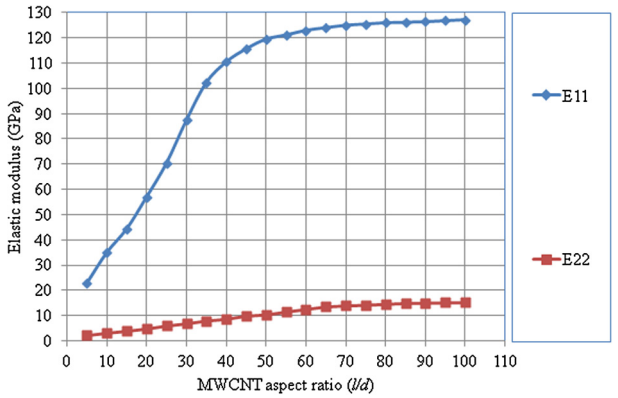

Fig. 16. (Color online.) Variation of Young's moduli E_{11} and E_{22}, with the aspect ratio (l/d) of armchair MWCNT-reinforced PC composite with fixed volume fraction $(V_f = 0.04)$.

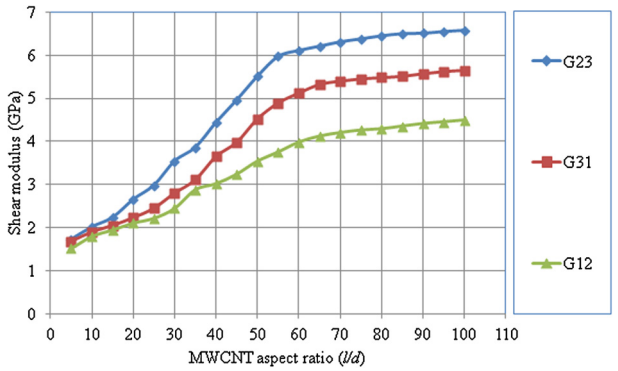

Fig. 17. (Color online.) Variation of the shear moduli with the aspect ratio (l/d) of armchair MWCNT-reinforced PC composite with fixed volume fraction $(V_f = 0.04)$.

in modulus later on when the MWCNT volume fraction increases by 6–16 %. The curvy and slippery nature of MWCNTs causes the shear modulus to decrease when increasing the MWCNT volume fraction. Moreover, Table 7 also shows that the percentage increase in shear moduli of the zigzag MWCNT-reinforced PC composite is greater than the percentage increase in the shear moduli of chiral MWCNT-reinforced PC composites. Comparing Table 6 and Table 7, it can be concluded that the percentage increase in shear moduli is smaller in comparison to the percentage increase in longitudinal elastic modulus. Thus, MWCNT-reinforced PC composites are weaker in shear than in other modes of loading.

Fig. 16 shows the variation of Young's moduli E_{11} and E_{22} with the aspect ratio (l/d) of armchair MWCNT-reinforced PC composite with volume fraction $(V_f = 0.04)$. When increasing the MWCNT aspect ratio (l/d) till $l/d = 50$, both the longitudinal and transverse elastic moduli increase rapidly. Thereafter, the increase is smaller. When the length of the CNTs increases, the efficiency of load transfer is increased dramatically. But for larger lengths, the increase in van der Waals forces causes the modulus to increase at a slower rate, as can be observed from Fig. 16. Fig. 17 shows the variation of the shear modulus with the aspect ratio (l/d) of armchair MWCNT-reinforced PC composites with a fixed volume fraction $(V_f = 0.04)$. It can be inferred that the increase in shear moduli is significantly smaller in comparison to the increase in longitudinal and transverse elastic moduli. All the shear moduli increase till $l/d = 50$. After that, the rise is minimal, which may be due to the increase in the van der Waals force for higher aspect ratios. Fig. 17 also shows that the increase in G_{31} and G_{12} is smaller than the increase in G_{23}.

Table 8 shows the percentage increase in elastic moduli when increasing the MWCNT aspect ratio (l/d) for a fixed volume fraction $(V_f = 0.04)$. From Fig. 16 and Table 8, it can be concluded that E_{11} and E_{22} increase sharply from $l/d = 5$

Table 8
Percentage increase in elastic modulus when increasing the MWCNT aspect ratio (l/d).

MWCNT aspect ratio (l/d)	Percentage increase in E_{11}	Percentage increase in E_{22}
5–50	418.07	381.56
50–100	6.43	46.41

Table 9
Percentage increase in shear moduli when increasing the MWCNT aspect ratio (l/d).

MWCNT aspect ratio (l/d)	Percentage increase in G_{23}	Percentage increase in G_{31}	Percentage increase in G_{12}
5–50	220.34	169.04	132.89
50–100	19.42	25.00	26.83

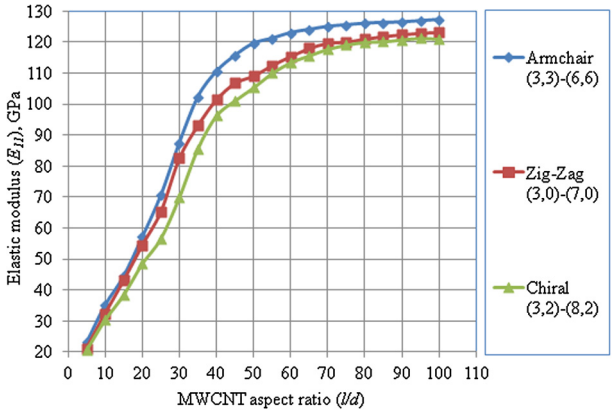

Fig. 18. (Color online.) Variation of the longitudinal modulus (E_{11}) with the aspect ratio (l/d) for different configurations of the MWCNT-reinforced PC composite with fixed volume fraction ($V_f = 0.04$).

to $l/d = 50$. A possible reason for this is the presence of shear stress concentration at numerous fiber ends in a short fiber composite. However, for $l/d > 50$, both moduli increase slowly. This is because, after $l/d = 50$, higher fiber axial stress occurs, which causes the moduli to increase at a slower rate.

Table 9 shows the percentage increase in shear moduli when increasing the MWCNT aspect ratio (l/d). It shows that the percentage increase in all the shear moduli is greater when the aspect ratio varies from $l/d = 5$ to $l/d = 50$. This is probably due to the fact that at low fiber aspect ratio, the number of fibers in the composite will be more for the same volume fraction. The higher the number of discontinuous fibers is, the higher the number of fiber-ends available for stress concentration is.

Thus, at low values of l/d, the stress concentration at numerous fiber ends leads to a rise in the values of all the shear moduli. As the fiber aspect ratio increases, shear moduli become constant, as shown in Fig. 17.

Fig. 18 shows the variation of the longitudinal modulus (E_{11}) with the aspect ratio (l/d) for different configurations of MWCNT-reinforced PC composites with fixed volume fraction ($V_f = 0.04$). It can be observed that armchair MWCNT-reinforced PC composites have a higher elastic modulus E_{11}, in comparison to zigzag and chiral MWCNT-reinforced PC composites. E_{11} increases rapidly till $l/d = 50$, after which the increase takes place at a slower rate. Due to the geometric orientation of the carbon–carbon bonds relative to the nanotube axis, armchair MWCNT-reinforced PC composite exhibit higher Young's moduli values compared to the zigzag MWCNT-reinforced PC composites. Chiral MWCNT-reinforced PC composites have lower elastic moduli because of the curved nature of all C=C sp^2 bonds. At lower values of l/d, the stress concentration at numerous fiber ends leads to a rise in the values of all the shear moduli.

Fig. 19 shows the variation of transverse modulus (E_{22}) with the aspect ratio (l/d) for different configurations of MWCNT-reinforced PC composites with a fixed volume fraction ($V_f = 0.04$). It can be observed here also that armchair MWCNT-reinforced PC composites have higher elastic modulus E_{22} in comparison to zigzag and chiral MWCNT-reinforced PC composites. It is inferred by comparing Figs. 18 and 19 that the values of E_{22} are significantly smaller than the corresponding values of E_{11}. This is because MWCNTs are aligned in the direction of the applied strain.

Fig. 20 shows the variation of the shear modulus (G_{23}) with the aspect ratio (l/d) for different configurations of MWCNT-reinforced PC composites with fixed volume fraction ($V_f = 0.04$). Armchair MWCNT-reinforced PC composites have higher shear moduli in comparison to zigzag and chiral MWCNT-reinforced PC composites. G_{23} increases rapidly till $l/d = 50$, after which the increase occurs at a slower rate.

Fig. 21 shows the Variation of the shear modulus (G_{31}), with the aspect ratio (l/d) for different configurations of MWCNT-reinforced PC composites with fixed volume fraction ($V_f = 0.04$). G_{31} increases rapidly till $l/d = 50$. After that, the rise is

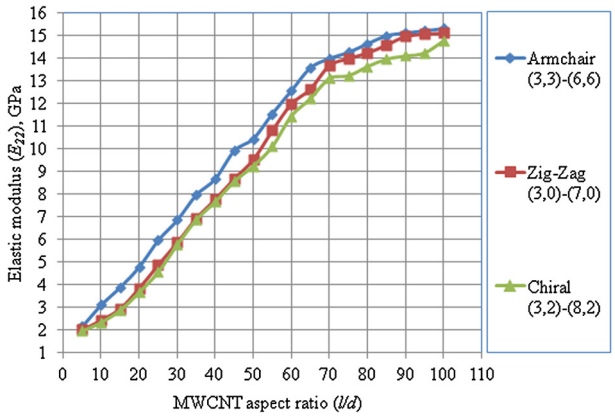

Fig. 19. (Color online.) Variation of the transverse modulus (E_{22}) with the aspect ratio (l/d) for different configurations of the MWCNT-reinforced PC composite with fixed volume fraction ($V_f = 0.04$).

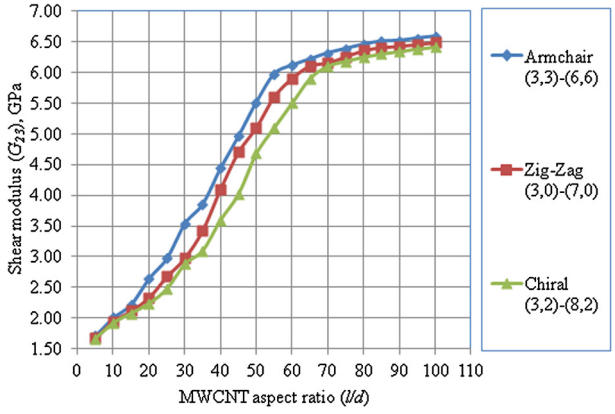

Fig. 20. (Color online.) Variation of the shear modulus (G_{23}) with the aspect ratio (l/d) for different configurations of the MWCNT-reinforced PC composite with fixed volume fraction ($V_f = 0.04$).

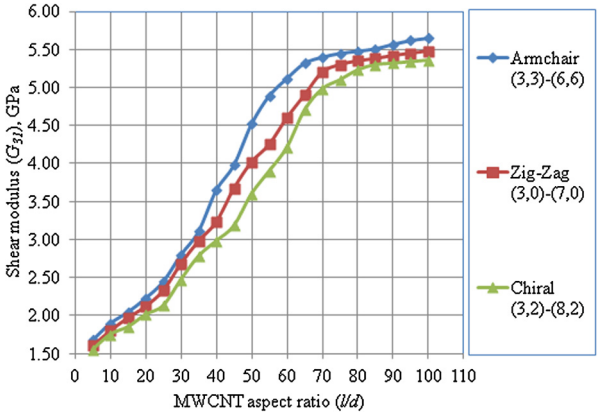

Fig. 21. (Color online.) Variation of the shear modulus (G_{31}) with the aspect ratio (l/d) for different configurations of the MWCNT-reinforced PC composite with fixed volume fraction ($V_f = 0.04$).

minimal, which may be due to the increase in van der Waals force for higher aspect ratios. Fig. 22 shows the variation shear modulus (G_{12}) with the aspect ratio (l/d) for different configurations of MWCNT-reinforced PC composites with a fixed volume fraction ($V_f = 0.04$). The trend is similar to that of G_{23}.

Table 10 shows the percentage increase in elastic moduli when increasing the MWCNT aspect ratio (l/d) for fixed volume fraction ($V_f = 0.04$). From Figs. 18–19 and Table 10, it can be observed that the percentage increase in elastic moduli is greater for MWCNT aspect ratio ($l/d = 5$ to $l/d = 50$) than the percentage increase in elastic moduli when $l/d = 50$ to

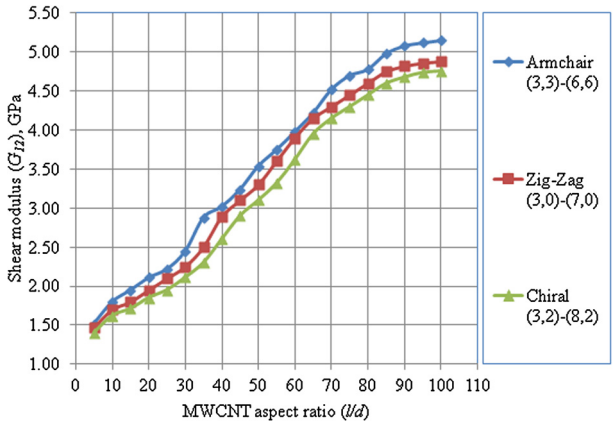

Fig. 22. (Color online.) Variation of the shear modulus (G_{12}) with the aspect ratio (l/d) for different configurations of MWCNT-reinforced PC composite with fixed volume fraction ($V_f = 0.04$).

Table 10
Percentage increase in elastic moduli when increasing the MWCNT aspect ratio (l/d).

MWCNT aspect ratio (l/d)	Increase in moduli (in %)					
	Armchair		Zigzag		Chiral	
	E_{11}	E_{22}	E_{11}	E_{22}	E_{11}	E_{22}
5–50	418.07	381.56	413.94	371.78	411.85	369.54
50–100	6.43	46.41	12.84	58.55	14.87	59.56

Table 11
Percentage increase in shear moduli when increasing the MWCNT aspect ratio (l/d).

MWCNT aspect ratio (l/d)	Increase in moduli (in %)								
	Armchair			Zigzag			Chiral		
	G_{23}	G_{31}	G_{12}	G_{23}	G_{31}	G_{12}	G_{23}	G_{31}	G_{12}
5–50	220.34	169.04	132.89	203.57	151.25	124.48	180.24	132.25	121.42
50–100	19.42	25.00	45.48	27.05	36.81	47.87	36.96	48.88	53.54

$l/d = 100$. Table 11 shows the percentage increase in shear moduli when increasing the MWCNT aspect ratio (l/d). It shows that the percentage increase in all the shear moduli is greater when the aspect ratio varies from $l/d = 5$ to $l/d = 50$. This is probably due to the fact that at low fiber aspect ratios, the number of fibers in the composite will be more for the same volume fraction. The higher the number of discontinuous fibers is, the higher the number of fiber-ends available for stress concentration is. Thus, at low values of l/d, the stress concentration at numerous fiber ends leads to a rise in the values of all the shear moduli. As the fiber aspect ratio increases, the shear moduli become constant, as shown in Figs. 20–22.

5.2. Damping

While most of the researches on nanocomposites with carbon nanotubes focus on elastic properties, relatively little effort to date has been put in the studies of their damping characteristics. In fact, there exists a great potential in developing nanocomposites with high damping capacity using carbon nanotubes, since the interfacial slips between nanotubes and polymer resin and between nanotubes themselves are believed to be significant. This is due to the nanoscale dimensions and the high aspect ratio of nanotubes, which results in a large interfacial contact area and high friction energy dissipation during the sliding of nanotube surfaces within the composite. To model a nanocomposite, molecular dynamics (MD) methods are often used.

Buldum and Lu [19] investigated the interfacial sliding and rolling of carbon nanotubes using MD methods. It was found that a nanotube first stick and then slips suddenly when the force exerted on it is sufficiently large. Suhr et al. [20] investigated the damping characteristics of polymers reinforced with multi-walled nanotubes and concluded that the stick-slip motion between the nanotubes themselves is believed to be the major contribution to the overall damping of the nanocomposite material. Because of the small size of nanotubes, the surface area to mass ratio (specific surface area) of carbon nanotube arrays is extremely large. Therefore, in composites with CNT fillers, it is anticipated that high damping can be achieved by taking advantage of the weak bonding and interfacial friction between individual CNTs and resin.

In this study, damping properties of carbon MWCNT/PC composites have been expressed analytically from the theory of short fiber composites. The elastic–viscoelastic correspondence principle—"a linear elastostatic analysis can be converted to

Table 12
Dynamic properties of MWCNTs and PC.

Dynamic properties	MWCNT	Polycarbonate
Storage modulus (E'), GPa	1000 (Esawi and Farag [26])	2.9 (Kumar et al. [11])
Loss modulus (E''), GPa	1.5	1.0
Loss factor (η)	0.0015	0.345
MWCNT volume fraction (V_f)	0.02	

a vibratory linear visco-elastic analysis by replacing the elastic moduli with the corresponding complex moduli"—has been used to define the dynamic properties. The complex modulus has a real and an imaginary part. The damping loss factor can be expressed as the ratio of the imaginary to the real part of the complex modulus.

$$\eta = \frac{C''}{C'} \tag{9}$$

where

$C^* = C' + \mathrm{i}C''$ = complex modulus of the composite
C' = storage modulus of the composite
C'' = loss modulus of the composite
η = damping loss factor of the composite.

By combining the self-consistent approach of Hill [21] with the solutions of Hermans [22] and making a few additional assumptions, Halpin and Kardos [17] provide a simpler analytical form for predicting material properties of fiber composites. Halpin–Tsai equations need only one equation to find all the composite moduli and the longitudinal Poisson's ratio is simply found from the rule of mixtures.

The dynamic properties of MWCNTs and polycarbonate matrix as given by Khatua et al. [23] are used as input and shown in Table 12.

Tandon and Weng [24] derived explicit expressions for the elastic constants of a short fiber composite using the Mori–Tanaka approach. Their formulae for the plane-strain bulk modulus k_{23} and the major Poisson ratio ν_{12} are coupled, and must be solved iteratively. Using Tandon and Weng [24] equations, Eshelby's tensor **E** is evaluated and further used in Eq. (10) to find the strain concentration tensor **A**. The strain concentration tensor is then used in Eq. (11) to find the stiffness and damping of the composite.

$$A^{\text{Eshelby}} = \left[I + ES^{\text{m}}\left(C^{\text{f}} - C^{\text{m}}\right)\right]^{-1} \tag{10}$$

$$C = C^{\text{m}} + V_{\text{f}}\left(C^{\text{f}} - C^{\text{m}}\right)A^{\text{Eshelby}} \tag{11}$$

where

V_f = fiber volume fraction
C^m = stiffness matrix of PC matrix
C^f = stiffness matrix of MWCNT
A^{Eshelby} = strain concentration tensor

By writing a program in Matlab, we can solve the equations and can study the effect of various parameters such as aspect ratio and fiber volume fraction on loss modulus, storage modulus and damping loss factor. Forcite mechanical properties calculations use the "Constant strain" approach. The process starts by removing symmetry from the system, followed by an optional re-optimization of the structure, where the cell parameters can be varied. Optimization at this stage is always advised, as incorrect results can be obtained if the structure is far from its lowest energy configuration. For each configuration, a number of strains are applied, resulting in a strained structure. The resulting structure is then optimized, keeping the cell parameters fixed. For example:

number of steps for each strain = 4
max. strain amplitude = 0.003
strain patterns 100000, 010000

This defines a range of values $\{-0.003, -0.001, 0.001, 0.003\}$, which are applied to each strain pattern:

strain pattern 100000 gives $e = \{-0.003, 0, 0, 0, 0, 0\}, \{-0.001, 0, 0, 0, 0, 0\}, \{0.001, 0, 0, 0, 0, 0\}, \{0.003, 0, 0, 0, 0, 0\}$
strain pattern 010000 gives $e = \{0, -0.003, 0, 0, 0, 0\}, \{0, -0.001, 0, 0, 0, 0\}, \{0, 0.001, 0, 0, 0, 0\}, \{0, 0.003, 0, 0, 0, 0\}$

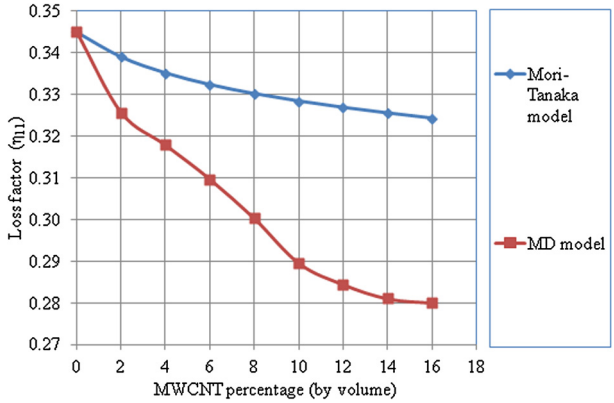

Fig. 23. (Color online.) Variation of loss factor (η_{11}) with the percentage of armchair MWCNT (by volume) in PC.

Table 13
Percentage variation in loss factor (η_{11}) when increasing the MWCNT volume fraction.

MWCNT (volume %)	Percentage difference in loss factor (η_{11}) w.r.t. previous value using MD	Percentage difference between Mori–Tanaka model and MD
0	–	–
2	5.57	3.91
4	2.58	5.14
6	2.39	6.81
8	2.03	9.05
10	1.86	11.81
12	1.76	12.96
14	1.19	13.62
16	0.35	13.64

Each strain pattern represents the strain matrix in Voigt notation. It is converted into the strain matrix **E**, such that $E(0,0) = e(0)$, $E(1,1) = e(1)$, $E(2,2) = e(2)$, $E(2,1) = E(1,2) = 0.5 \times e(3)\ldots$

These are then used to generate the metric tensor **G**:

$$\mathbf{G} = \mathrm{H0}'[2\mathrm{E} + \mathrm{I}]\mathrm{H0}$$

where H0 is formed from the lattice vectors; I is the identity matrix and H0′ is the transpose of H0. The new lattice parameters can be derived from **G**; these are then used to transform the cell parameters (fractional coordinates are held fixed). Following these steps, the structure is optimized and the stress is calculated. A stiffness matrix is built up by from a linear fit between the applied strain and the resulting stress patterns. In the case of a trajectory, this is averaged over all frames.

In Materials Studio 5.5, the energy dissipated can be obtained after completion of the mechanical property calculation task. From the "Forcite" mechanical properties task, we get two values of energy. Energy in frame 1 gives that during loading, whereas energy in frame 2 gives the energy during unloading cycle. Area between loading and unloading curves gives us the energy dissipated. Dividing this dissipated energy by the energy obtained before the unloading cycle begins gives the measure of damping (η). Results of MD have been compared with the results obtained from the Mori–Tanaka model (Eq. (11)).

Fig. 23 shows the variation of the loss factor (η_{11}) with the percentage of armchair MWCNT (by volume) in PC. It shows that the loss factor (η_{11}) decreases when increasing the MWCNT volume fraction. The percent decrease in η_{11} when increasing the MWCNT volume fraction is shown in Table 13. From Fig. 23 and Table 13, it can be observed that η_{11} decreases sharply till the MWCNT volume fraction is 2%. Thereafter, the fall steadies due to the aggregation of MWCNTs and the curvy and slippery nature of MWCNTs do not assist in a further decline of damping properties. It can also be observed that the difference between the Mori–Tanaka model and the MD model goes on increasing as the volume fraction increases.

Fig. 24 shows the variation of the loss factor (η_{11}) with the percentage of MWCNT (by volume) in PC, for different configurations of MWCNT. All the simulations were performed with the MWCNT aspect ratio ($l/d = 10$). The carbon atoms in a CNT are in sp^2 configurations and connected to one another by three strong σ bonds. Due to the geometric orientation of the carbon–carbon bonds relative to the nanotube axis, armchair MWCNT-reinforced PC composites exhibit higher Young's moduli values compared to zigzag MWCNT-reinforced PC composites. Since the loss factor is inversely proportional to Young's modulus, therefore armchair MWCNT-reinforced PC composites exhibit lowest damping values. Chiral MWCNT-reinforced PC composites have highest loss factor because of the curved nature of all C=C sp^2 bonds.

Table 14 shows the percentage decrease in loss factor when increasing the MWCNT volume fraction. From Fig. 24 and Table 14, it can be inferred that initially, when increasing the MWCNT volume fraction by 0–6%, the fall in η_{11} is faster

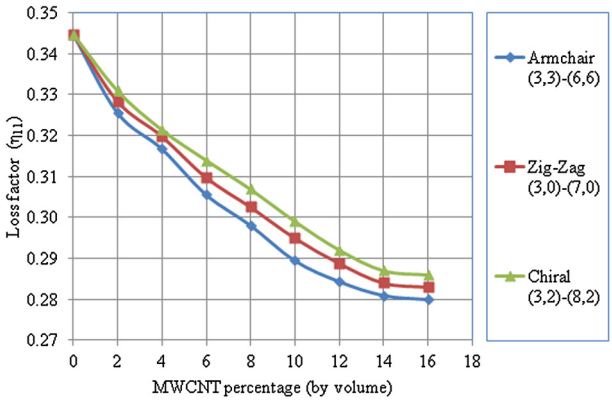

Fig. 24. (Color online.) Variation of loss factor (η_{11}) with the percentage of MWCNT (by volume) in PC, for different configurations of MWCNT.

Table 14
Percentage decrease in loss factor when increasing the MWCNT volume fraction.

MWCNT range (volume %)	Decrease in loss factor (in %)		
	Armchair	Zigzag	Chiral
0–6	11.37	10.15	8.93
6–16	8.37	8.64	8.91

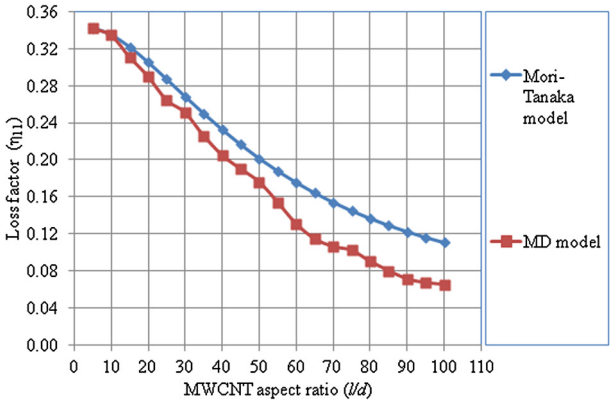

Fig. 25. (Color online.) Variation of loss factor (η_{11}) with the aspect ratio (l/d) of armchair MWCNT-reinforced PC composites with fixed volume fraction ($V_f = 0.04$).

Table 15
Percentage decrease in loss factor (η_{11}) when increasing the MWCNT aspect ratio (l/d).

MWCNT aspect ratio (l/d)	Percentage decrease in η_{11}	Percentage difference between Mori–Tanaka model and MD model at		
		$l/d = 5$	$l/d = 60$	$l/d = 100$
5–60	61.75	0.28	25.54	41.30
60–100	50.26			

when compared with the fall in modulus later on. Fig. 25 shows the variation of the loss factor (η_{11}) with the aspect ratio (l/d) of the armchair MWCNT-reinforced PC composite with fixed volume fraction ($V_f = 0.04$). When increasing the MWCNT aspect ratio (l/d) till $l/d = 60$, the longitudinal loss factor decreases rapidly. Thereafter, the decrease is smaller. When the length of the CNTs increases, the efficiency of load transfer is increased dramatically. But for larger lengths, the increase in van der Waals force causes the loss factor to decrease at a slower rate. The Mori–Tanaka model gives higher values of the loss factor (η_{11}) than MD.

Table 15 shows the percentage decrease in η_{11} when increasing the MWCNT aspect ratio (l/d) for a fixed volume fraction ($V_f = 0.04$). From Fig. 25 and Table 15, it can be concluded that η_{11} decreases sharply from $l/d = 5$ to $l/d = 60$. A possible reason for this is the presence of shear stress concentration at numerous fiber ends in a short fiber composite. However, for $l/d > 60$, η_{11} decreases slowly. This is because, after $l/d = 60$, higher fiber axial stress occurs, which causes the loss factor

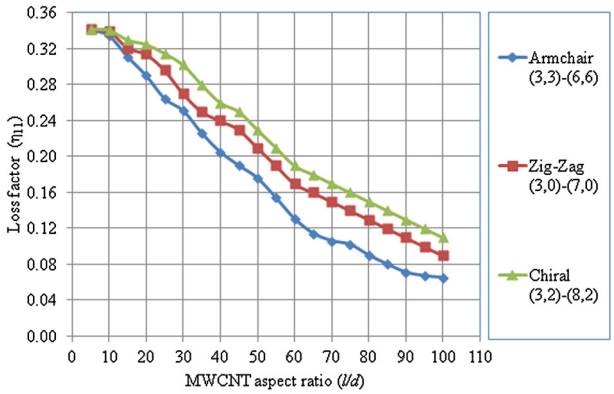

Fig. 26. (Color online.) Variation of loss factor (η_{11}) with the aspect ratio (l/d) for different configurations of MWCNT-reinforced PC composites with fixed volume fraction ($V_f = 0.04$).

Table 16
Percentage decrease in loss factor (η_{11}) when increasing the MWCNT aspect ratio (l/d).

MWCNT aspect ratio (l/d)	Decrease in η_{11} (in %)		
	Armchair	Zigzag	Chiral
5–60	61.75	50.26	44.46
60–100	50.26	47.05	42.10

to decrease at a slower rate. It can also be observed that at low aspect ratios, the Mori–Tanaka model and MD give almost similar results. At $l/d = 5$, the percentage difference between them is only 0.28%.

Fig. 26 shows the variation of the loss factor (η_{11}) with the aspect ratio (l/d) for different configurations of MWCNT-reinforced PC composites with fixed volume fraction ($V_f = 0.04$). It can be observed that armchair MWCNT-reinforced PC composites exhibit lower values of loss factor (η_{11}), in comparison to zigzag and chiral MWCNT-reinforced PC composites. η_{11} decreases rapidly till $l/d = 60$, after which the decrease takes place at a slower rate. Due to the geometric orientation of the carbon–carbon bonds relative to the nanotube axis, the armchair MWCNT-reinforced PC composites exhibit higher Young's moduli values compared to zigzag MWCNT-reinforced PC composites. Chiral MWCNT-reinforced PC composites have lower elastic moduli because of the curved nature of all C=C sp^2 bonds. Since the loss factor is inversely proportional to Young's modulus, therefore armchair MWCNT-reinforced PC composites exhibit lowest damping values.

Table 16 shows the percentage decrease in η_{11} when increasing the MWCNT aspect ratio (l/d) for a fixed volume fraction ($V_f = 0.04$). From Fig. 26 and Table 16, it can be observed that the percentage decrease in η_{11} is greater for the MWCNT aspect ratio ($l/d = 5$ to $l/d = 60$) than the percentage decrease in η_{11} when $l/d = 60$ to $l/d = 100$. Because armchair MWCNT-reinforced PC composites exhibit the highest elastic moduli, therefore they have the lowest damping values.

There are two possible mechanisms that could be responsible for damping in MWCNT-reinforced polymer composites at the molecular level: (a) energy dissipation caused by interfacial sliding at the nanotube–polymer interface, and (ii) energy dissipation caused by interfacial stick-slip sliding at the nanotube–nanotube interface. When a normal tensile stress is applied to a composite, it starts elongating. As a result of the applied stress, the resin starts applying a shear stress on the nanotube, thus causing the load to be transferred to nanotubes. Consequently, normal strain starts appearing in nanotubes and they start elongating accordingly. When the applied stress is small, the nanotube remains bonded to the matrix (sticking phase). Both the resin and the nanotube move together during this phase and the strains are equal in both epoxy resin and nanotube. As the applied stress is increased, the shear stress on CNT increases. At a certain value of shear stress, called the critical shear stress, the nanotube debonds from the resin. When the shear stress on the nanotube increases beyond this value (as a result of increased applied stress), the epoxy starts flowing over the surface of the nanotube.

The strain in the nanotube remains constant at its maximum level while the strain in the epoxy increases (slipping phase). In this phase, there is no transfer load between CNT and matrix, and because of this energy dissipation due to slippage occurs, which results in structural damping.

5.3. Thermal conductivity

Thermal conductivity results obtained using MD simulations were compared with other models such as series model, parallel model, Maxwell–Garnett model, Lewis–Nielsen model, and Hamilton–Crosser model. Comparison of MD results for the variation of thermal conductivity with MWCNT aspect ratio was made with Deng's model. Fig. 27 shows the temperature profile generated while calculating the thermal conductivity for MWCNT–PC composite with $V_f = 0.10$ and $l/d = 10$. Fig. 28 shows the variation of thermal conductivity with time for MWCNT–PC composite with $V_f = 10\%$. It shows that the value of thermal conductivity stabilizes after approximately 60 ps.

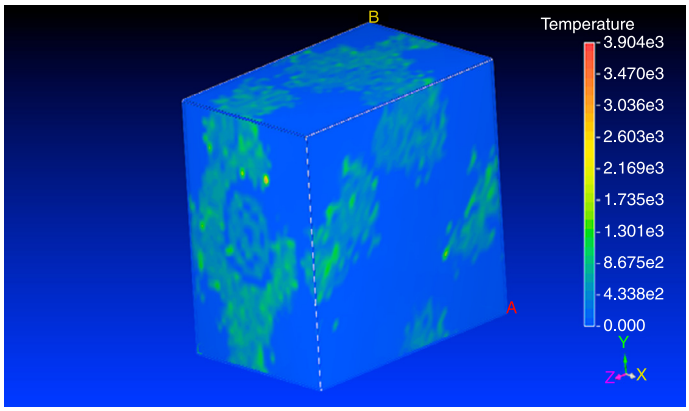

Fig. 27. (Color online.) Temperature profile generated while calculating thermal conductivity for MWCNT–PC composites with $V_f = 10\%$.

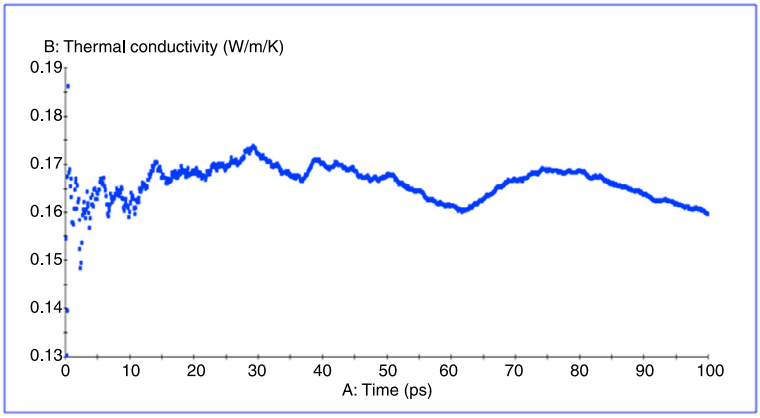

Fig. 28. (Color online.) Variation of the thermal conductivity with time for MWCNT–PC composites with $V_f = 10\%$.

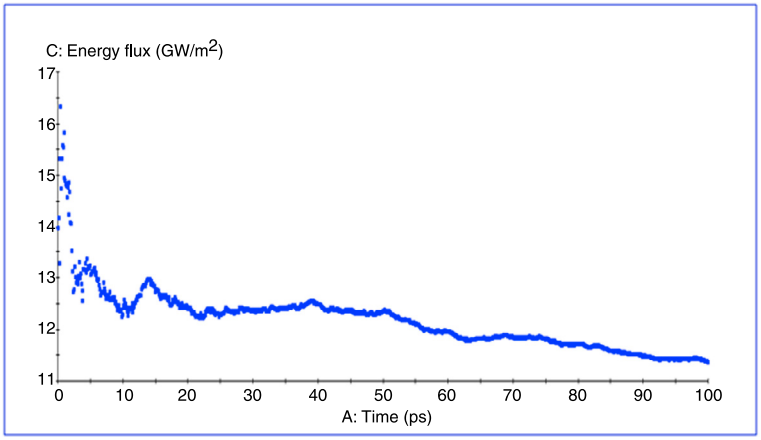

Fig. 29. (Color online.) Variation of the energy flux with time for MWCNT–PC composites with $V_f = 10\%$.

Fig. 29 shows the variation of energy flux with time for MWCNT–PC composite with $V_f = 10\%$. It shows that the value of energy flux stabilizes after approximately 60 ps. The size of the MWCNTs and their shape play an important role in the heat transfer between polymer matrix and the incorporated filler. Fillers with a higher thermal conductivity than PC improve the heat transfer of composites—one can consider that PC is a thermal barrier for heat propagation—while the filler material transmits the heat much faster. The thermal conductivity of nanocomposites might have a completely different mechanism in contrast to micro-composites. In the case of micro-composites, the heat is transported by micro-fibers much faster than in PC.

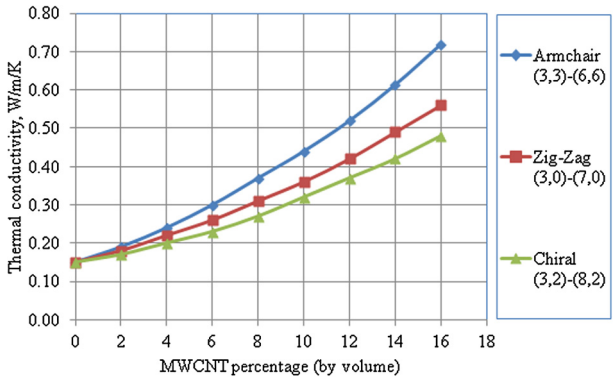

Fig. 30. (Color online.) Variation of the thermal conductivity with the volume fraction for different types of MWCNTs with fixed aspect ratio ($l/d = 10$).

Phonons, which are responsible for heat conduction in dielectric materials, are scattered at the interface between dissimilar materials. The heat dissipates on the surface of nano-fibers to a higher degree than on the surface of micro-fibers. In the case of nanocomposite systems with a surface-modified filler, heat transport is controlled by the interface provided by a coupling agent that connects inorganic particles on one side and the polymer host on the other side. When nanosized fillers are used, the relative surface area of the interface, and thus the volume of the interfacial zone, is significant. Hence, the interfacial zone will determine the thermal conductivity of the system, since it can conduct heat much better than the constituents themselves. This means that ultimately the thermal conductivity is affected more by the interfacial zone than by the polymer and nano-fibers.

When assembling CNTs into large-scale composites, it is difficult to make full use of the excellent thermal conductivity of individual CNTs (3000 W/m K). Weak tube–tube coupling, dangling tube ends, misalignment and structural defects all contribute to quenching of phonon modes and thus decrease the thermal conductivity of the composites. Longer and thicker CNT would amount to a more efficient heat conduction path, which also allows the transport of phonons with longer wavelengths. In addition, larger-diameter MWCNTs are more likely to form a rigid and compact structure and thus reduce the thermal contact resistance at the intertube and tube-polymer interfaces.

For short nanotube-reinforced composites, the phonon mobility is restricted at the interface as a result of the thermally insulating nature of the polymer. In such case, the overall thermal conductivity is mechanistically limited by the high CNT/polymer interfacial thermal resistance. The prerequisite for investigating CNT length effect on thermal conductivities of composites is a near-ideal structure of the composites. Factors including CNT length, volume fraction, alignment and contact area all contribute to the efficiency of phonon transport in the composites.

Since the mechanism of heat conduction by phonons or electrons depends profoundly on the band gaps of materials, the heat transfer mechanism of CNTs is found to depend strongly on the chirality, which determines the size of their band gaps and electronic properties. The largest band gap (on the order of 1.5 eV) is found in nanotubes with (n, m) chiral indices defining the chiral vector satisfying the condition: $|n - m| \neq 3p$, where p is an integer. For other types of nanotubes, the band gap is considerably smaller in the case of armchair nanotubes ($n = m$). Thus, the electronic contribution to the thermal conductivity will be significant in metallic CNTs with a small band gap. On the other hand, thermal conductivity of chiral CNT is mainly governed by the phonon component.

Fig. 30 shows the variation of thermal conductivity with the volume fraction of different types of MWCNTs with fixed aspect ratio ($l/d = 10$). It can be observed that armchair MWCNT-reinforced PC composites exhibit the highest thermal conductivity and the chiral MWCNT-reinforced PC composites have the lowest thermal conductivity amongst all the configurations of MWCNT. Because of the large band gap in chiral MWCNTs, the composites reinforced with these tubes display poor thermal conductivity, as can be observed from Fig. 30. The thermal conductivity increases when increasing the volume of MWCNTs. It is because of the excellent thermal conductivity of MWCNTs that the conductivity of MWCNT-reinforced PC composites increases significantly.

Table 17 shows the percentage increase in thermal conductivity with V_f for armchair MWCNT–PC composite using MD. It shows that the thermal conductivity of armchair MWCNT-reinforced PC composite increases approximately by 380% when increasing the MWCNT volume fraction from 0 to 16%. Table 18 shows the percentage difference in thermal conductivity for different configurations of MWCNT-reinforced PC composites. It shows that the difference in thermal conductivity between the armchair and other type of MWCNTs increases as V_f increases. This is due to the large band gap for zigzag and chiral MWCNTs in comparison with armchair MWCNTs. Moreover, the percentage difference between armchair MWCNT-reinforced and zigzag MWCNT-reinforced PC composites is smaller in comparison to the percentage difference between armchair MWCNT-reinforced and chiral MWCNT-reinforced PC composite.

Fig. 31 shows the comparison of MD results of thermal conductivity for armchair MWCNT-reinforced PC composite with other models with fixed aspect ratio ($l/d = 10$). Thermal conductivity shows an increasing trend when increasing MWCNT volume fraction. The series model and the parallel model both assume that each phase contribute independently to the overall thermal resistance and conductance, respectively, and assume a perfect interface between any two phases in contact.

Table 17
Percentage increase in thermal conductivity with V_f for an armchair MWCNT–PC composite using MD.

MWCNT V_f (in %)	Thermal conductivity (W/m/K)	Percentage increase w.r.t. previous value	Percentage increase w.r.t. $V_f = 0$
0	0.15	–	–
2	0.19	26.66	26.66
4	0.24	26.31	60.00
6	0.30	25.00	100.00
8	0.37	23.33	146.66
10	0.44	18.91	193.33
12	0.52	18.18	246.66
14	0.61	18.07	309.33
16	0.72	17.26	380.00

Table 18
Percentage difference in thermal conductivity for different configurations of MWCNT-reinforced PC composites.

MWCNT V_f (in %)	Percentage difference in thermal conductivity	
	Between armchair MWCNT-reinforced and zigzag MWCNT-reinforced PC composites	Between armchair MWCNT-reinforced and chiral MWCNT-reinforced PC composites
0	0	0
2	5.26	10.52
4	8.33	16.66
6	13.33	23.33
8	16.21	27.02
10	18.18	27.27
12	19.23	28.84
14	20.19	31.59
16	22.22	33.33

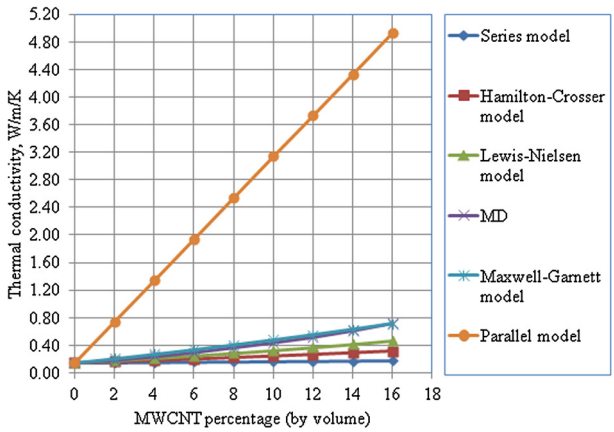

Fig. 31. (Color online.) Comparison of MD results of thermal conductivity for armchair MWCNT-reinforced PC composites with other models with fixed aspect ratio ($l/d = 10$).

However, it typically gives an underestimation for a particulate composite due to the presumably complete localization of the contribution from the particles embedded in the matrix, that is, neglecting the interaction among the fillers. Therefore, the series model gives the lower bound for thermal conductivity of composites. In comparison, the parallel model predicts the thermal conductivity of conventional continuous fiber-reinforced composites along the fiber-alignment direction. For composites with fibrous inclusions, the rule of mixture implicitly assumes perfect contact between particles in a fully percolating network.

However, it gives a large overestimation of thermal conductivity for other types of composites, and gives an upper bound for the thermal conductivity of composites. It is important to point out that thermal conductivity measurement results of composites should always fall between the predictions of the series model (lower bound) and the parallel model (upper bound) except for the cases where interfacial phonon scattering in nano-laminates can yield even lower thermal conductivity than the lower bound by the series model.

Based on the continuity of potential and electric current at the interface, and on the assumption that the interactions among the spherical fillers are negligible, which means that the disseminated small spheres are located far enough from each other, Maxwell derived an analytical formula for the effective specific resistance (K) of "a compound medium consisting of a substance of specific resistance K_2, in which are disseminated small spheres of specific resistance K_1, the ratio of

Table 19
Comparison of MD results for thermal conductivity of armchair MWCNT-reinforced PC composite with other models.

MWCNT V_f (in %)	Percentage difference in thermal conductivity between	
	Maxwell–Garnett model and MD	MD and Lewis–Nielsen model
0	0	0
2	13.75	4.21
4	12.66	10.00
6	10.52	16.33
8	10.00	21.89
10	8.63	25.22
12	6.15	28.46
14	2.60	31.92
16	1.25	34.86

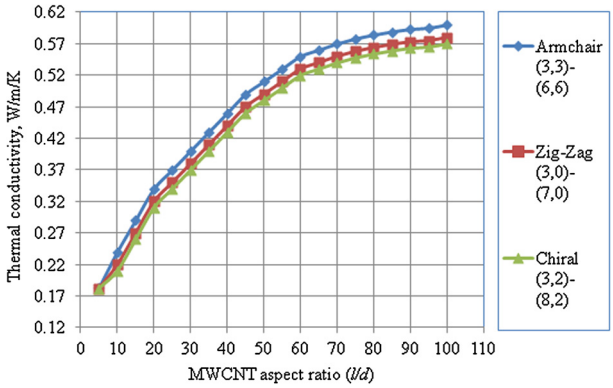

Fig. 32. (Color online.) Variation of the thermal conductivity with the aspect ratio (l/d) for different types of MWCNTs with fixed volume fraction ($V_f = 0.04$).

the volume of all the small spheres to that of the whole being p." This model gives satisfactory results for composites with: (i) spherical inclusions, (ii) very low V_f, (iii) good dispersion, and (iv) no interfacial thermal resistance. Since neither interfacial resistance nor particle–particle interaction was taken into account in the Hamilton–Crosser model, the fiber size was found to have no influence on the effective thermal conductivity of the composite in this model.

Although Nielsen's model is a semi-empirical model, at least three important improvements to the model should be appreciated. First, the shape effect and to some extent the orientation effect are both taken into account. Second, "reduced filler loading" accounts for the maximum packing density of the fillers with a specific shape and size distribution, and is unique to this model. In comparison, most of the theoretical equations assume uniform changes of filler loading up to the point where the dispersed phase makes up the complete system, which is not realistic. Third, the earliest definition of "effective unit" is reflected in the discussion on "aggregates of spheres".

Table 19 shows a comparison of MD results for thermal conductivity of armchair MWCNT-reinforced PC composites with other models. It can be inferred that at low MWCNT volume fractions, MD results agree well with the Lewis–Nielsen model. But at higher volume fractions, results of MD are in agreement with the Maxwell–Garnett model. Fig. 32 shows the variation of thermal conductivity with the aspect ratio (l/d) for different types of MWCNTs with fixed volume fraction ($V_f = 0.04$). Armchair MWCNT-reinforced PC composites exhibit the highest values of thermal conductivity for varying l/d and fixed V_f. Heat transport in MWCNT/PC composites is carried out by phonons of various wavelengths. CNT lengths are much longer than the mean free path of phonons. The effect of short-wavelength phonons probably reaches a stable level while long-wavelength phonons continue to contribute to the heat transport process. As a result, a longer CNT would amount to a more efficient heat conduction path, which also allows the transport of phonons with longer wavelengths. This results in an increase of thermal conductivity when increasing l/d.

Fig. 33 shows the variation of thermal conductivity of armchair MWCNT-reinforced PC composite with other models with fixed $V_f = 0.04$ and varying l/d. Longer CNTs with larger tubular diameter and more walls led to more efficient long-distance phonon and electron conductions, resulting in higher thermal conductivities in the composites. It can be inferred from Fig. 33 that at low MWCNT aspect ratios, MD results are in agreement with the results given by Deng model. However, after $l/d = 50$, the results of MD start deviating from those obtained by Deng model.

A large volume of literature reports the characterization of the PC-based materials by using a universal testing machine. However, Kumar et al. [11] used a nano-indenter that has also been used for the characterization of various other types of materials. However, there is no study available at a molecular dynamic level for MWCNT–PC composites, which can supplement the experimental findings. The composite materials used in this study comprise nano-sized fillers in the form of MWCNTs. Hence it becomes essential to study the properties of nano- or micro-scale owing to the size of the filler under observation and the properties at this level are complementary to the properties at the macro level.

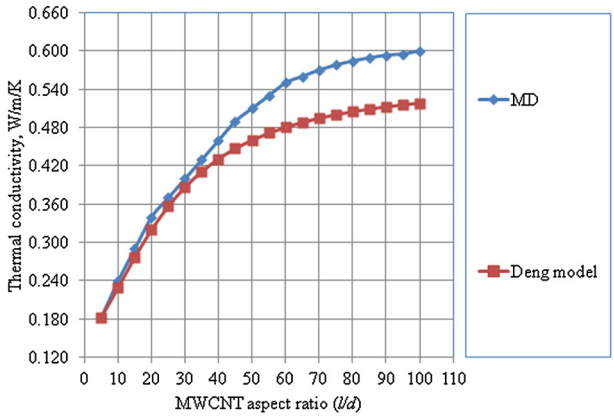

Fig. 33. (Color online.) Variation of the thermal conductivity of armchair MWCNT-reinforced PC composites with other models with fixed volume fraction $V_f = 0.04$.

In an earlier work by Jindal et al. [25], dynamic load tests on similar samples using Split Hopkinson Pressure Bar (SHPB) were reported, but the findings were somewhat different. It was found that for low concentrations of 0.5% MWCNTs, the increase in dynamic strength was most significant and remained almost the same up to 2% of MWCNTs, while for a higher concentration of 5% MWCNTs, this increase was negligible. The method used to determine the data based on SHPB was not dependent on a single-point measurement, but rather on a total effect on the whole cross section, and the extent of the applied load was much higher, which caused crushing of the specimen.

From the results of this paper, the elastic modulus, which is a measure of the stiffness of an elastic material and is a quantity used to characterize materials, increases when increasing the weight and the volume of MWCNTs. Considering a combined effect of both weight and volume studies, it is safe to state that 5% MWCNT composition in pure PC is the most suitable one to enhance the mechanical properties to a sufficient extent for any mechanical load and pressure-related application. Plastic deformation in amorphous polymers occurs due to nucleation and propagation of shear bands. In the unreinforced polymer matrix, shear bands propagate unchecked as there are no barriers for their movement. On the other hand, the presence of MWCNTs in the composites could offer resistance for the propagation of shear bands. The reasons for the enhancement of elastic modulus in polymer MWCNT nanocomposites are good mechanical interlocking and the presence of obstacles to the motion of shear bands.

6. Conclusions

The study presents results of MD simulation for elastic modulus obtained by using Materials Studio 5.5 and it supplements an earlier experimental study conducted by using a nano-indenter on a MWCNT-based PC composite. The results indicate unambiguously that static mechanical properties of pure PC are greatly enhanced by composing these with less than 10% of MWCNT. On the basis of the findings of this paper on the elastic properties of MWCNT–PC composites, it is safe to conclude that a concentration around 2% of MWCNT is a good compromise to form composites suitable for enhancing both static as well as dynamic properties. The main findings of the study are summarized as below:

(a) when the MWCNT weight percent increases from 0–5%, the percentage increase in E_{11} and E_{22} is greater than when the weight percent increases by 5–10%;
(b) our study supplements an earlier experimental study conducted by Kumar et al. [11] using a nano-indenter on a MWCNT based PC composite;
(c) with an increase in weight percent of MWCNT in PC, all the moduli show an increasing trend, but the increase in shear moduli is small;
(d) with only 2% addition by volume of MWCNT in PC, E_{11} increases by 925%. Thereafter, the increase occurs at a lower rate. The increase in E_{22} is much less than the increase in E_{11};
(e) armchair MWCNT-reinforced PC composites exhibit the highest values of moduli in comparison to zigzag and chiral MWCNT-reinforced PC composites;
(f) till $l/d = 50$, both longitudinal and transverse elastic moduli increase rapidly. Thereafter, the increase is smaller;
(g) the loss factor (η_{11}) decreases when increasing the MWCNT volume fraction. η_{11} decreases sharply till the MWCNT volume fraction is 2%. Thereafter, the fall steadies due to the aggregation of MWCNTs and the curvy and the slippery nature of MWCNTs do not assist in further decline of damping;
(h) chiral MWCNT-reinforced PC composites exhibit the highest values of damping in comparison to zigzag and armchair MWCNT-reinforced PC composites;

(i) when increasing the MWCNT aspect ratio (l/d) till $l/d = 60$, the longitudinal loss factor (η_{11}) decreases rapidly. Thereafter, the decrease is smaller. For larger lengths, the increase in van der Waals force causes the loss factor to decrease at a slower rate;
(j) because of the large band gap in chiral MWCNTs, the composites reinforced with these tubes display poor thermal conductivity. The thermal conductivity of composites increases when increasing the volume for all types of MWCNTs. The thermal conductivity increases approximately by 27% upon addition of only 2% by volume of MWCNTs;
(k) the results of thermal conductivity obtained from MD are in agreement with the Maxwell–Garnett and Lewis–Nielsen models;
(l) longer CNTs with larger tube diameter and more walls lead to more efficient long-distance phonon and electron conductions, resulting in higher thermal conductivities in the composites.

References

[1] M.F. Yu, O. Lourie, M. Dyer, K. Moloni, T.F. Kelly, R.S. Ruoff, Strength and breaking mechanism of multi walled carbon nanotubes under tensile load, Science 287 (5453) (2000) 637–640.
[2] W.S. Choi, R.S. Hun, Improvement of interfacial interaction via ATRP in polycarbonate/carbon nanotube nanocomposites, Colloids Surf. A 375 (1–3) (2011) 55–60.
[3] S.P. Liu, S.S. Hwang, J.M. Yeh, K.W. Pan, Enhancement of surface and bulk mechanical properties of polycarbonate through the incorporation of raw MWNTs-using the twin-screw extruder mixed technique, Int. Commun. Heat Mass Transf. 37 (7) (2010) 809–814.
[4] M. Olek, K. Kempa, S. Jurga, M. Giersig, Nanomechanical properties of silica-coated multiwall carbon nanotubes poly(methyl methacrylate) composites, Langmuir 21 (7) (2005) 3146–3152.
[5] B. Das, P.K. Eswar, U. Ramamurty, C.N.R. Rao, Nano-indentation studies on polymer matrix composites reinforced by few-layer graphene, Nanotechnology 20 (12) (2009) 125705–125710.
[6] S.R.C. Vivekchand, U. Ramamurty, C.N.R. Rao, Mechanical properties of inorganic nanowire reinforced polymer–matrix composites, Nanotechnology 17 (11) (2006) S344–S350.
[7] K.H. Kim, W.H. Jo, A strategy for enhancement of mechanical and electrical properties of polycarbonate/multi-walled carbon nanotube composites, Carbon 47 (4) (2009) 1126–1134.
[8] A. Eitan, F.T. Fisher, R. Andrews, L.C. Brinson, L.S. Schadler, Reinforcement mechanisms in MWCNT-filled polycarbonate, Compos. Sci. Technol. 66 (9) (2006) 1162–1173.
[9] M.R. Ayatollahi, S. Shadlou, M.M. Shokrieh, Fracture toughness of epoxy/multi-walled carbon nanotube nano-composites under bending and shear loading conditions, Mater. Des. 32 (4) (2011) 2115–2124.
[10] A. Montazeri, N. Montazeri, Viscoelastic and mechanical properties of multi walled carbon nanotube/epoxy composites with different nanotube content, Mater. Des. 32 (4) (2011) 2301–2307.
[11] N. Kumar, P. Jindal, M. Goyal, Mechanical characterization of multiwalled carbon nanotubes-polycarbonate composites, Mater. Des. 54 (1) (2014) 864–868.
[12] P.K. Schelling, S.R. Phillpot, P. Keblinski, Comparison of atomic-level simulation methods for computing thermal conductivity, Phys. Rev. B 65 (14) (2002) 144306–144317.
[13] M.S. Green, Markov random processes and the statistical mechanics of time dependent phenomenon, J. Chem. Phys. 20 (1) (1952) 1281–1295.
[14] R. Kubo, Statistical–mechanical theory of irreversible processes. I. General theory and simple applications to magnetic and conduction problems, J. Phys. Soc. Jpn. 12 (1957) 570–586.
[15] S. Lepri, R. Livi, A. Politi, Thermal conduction in classical low-dimensional lattices, Phys. Rep. 377 (1) (2003) 1–80.
[16] P. Jund, R. Jullien, Molecular dynamics calculation of the thermal conductivity of vitreous silica, Phys. Rev. B 59 (1999) 13707–13711.
[17] J.C. Halpin, J.L. Kardos, The Halpin–Tsai equations: a review, Polym. Eng. Sci. 16 (1976) 344–352.
[18] R.L. Hamilton, O.K. Crosser, Thermal conductivity of heterogeneous two-component systems, Ind. Eng. Chem. Fundam. 1 (3) (1962) 187–191.
[19] A. Buldum, J.P. Lu, Atomic scale sliding and rolling of carbon nanotubes, Phys. Rev. Lett. 83 (1999) 5050–5053.
[20] J. Suhr, N. Koratkar, P. Keblinski, P. Ajayan, Viscoelasticity in carbon nanotube composites, Nat. Mater. 4 (2005) 134–137.
[21] R. Hill, A self-consistent mechanics of composite materials, J. Mech. Phys. Solids 13 (1965) 213–222.
[22] J.J. Hermans, The elastic properties of fiber reinforced materials when the fibers are aligned, Proc. K. Ned. Akad. Wet., Ser. B, Phys. Sci. 65 (1967) 1–9.
[23] B. Khatua, N.K. Shrivastava, S. Maiti, A strategy for achieving low percolation and high electrical conductivity in melt-blended polycarbonate (PC)/multiwall carbon–nanotube (MWCNT) nanocomposites: electrical and thermo-mechanical properties, eXPRESS Polym. Lett. 7 (6) (2013) 505–518.
[24] G.P. Tandon, G.J. Weng, The effect of aspect ratio of inclusions on the elastic properties of uni-directionally aligned composites, Polym. Compos. 5 (1984) 327–333.
[25] P. Jindal, P. Shailaja, P. Sharma, V. Mangla, A. Chaudhury, D. Patel, B.P. Singh, R.B. Mathur, M. Goyal, High strain rate behavior of multi-walled carbon nanotubes–polycarbonate composites, Composites, Part B, Eng. 45 (1) (2013) 417–422.
[26] A.M.K. Esawi, M.M. Farag, Carbon nanotube reinforced composites: potential and current challenges, Mater. Des. 28 (9) (2007) 2394–2401.